Electronic Supplementary Information for

Lithium, Sodium, Potassium and Calcium Amine-bis(phenolate) Complexes in the Ring-opening Polymerization of *rac*-Lactide†

Katalin Devaine-Pressing,[a] Fabio Oldenburg,[a] Jan P. Menzel,[a] Maximilian Springer,[a] Louise N. Dawe,[b] and Christopher M. Kozak*,[a]

[a] Department of Chemistry, Memorial University of Newfoundland, St. John's, Newfoundland, A1B 3X7, Canada. E-mail: ckozak@mun.ca; Tel: +1-709-864-8082

[b] Department of Chemistry and Biochemistry, Wilfrid Laurier University, Waterloo, Ontario, N2L 3C5, Canada

X-ray crystallography

Crystallographic and structure refinement data of **3**·THF and **4** are given in Table S1. Single crystals of **3**·THF and **4** were mounted on a glass fibre using Paratone-N oil. For **3**·THF, all measurements were made on a Rigaku Saturn CCD area detector with a SHINE optic and graphite monochromated Mo-Kα radiation, for **4**, a graphite monochromated Mo-Kα radiation solved on an AFC8-Saturn 70 single crystal X-ray diffractometer from Rigaku, equipped with an X-stream 2000 low temperature system. Using Olex2,[1] the structure was solved with the ShelXT[2] structure solution program using Direct Methods and refined with the ShelXL[3] refinement package using Least Squares minimisation.

For **3**·THF, H2 was introduced in its difference map position and refined with Uiso = 1.5 Ueq of O2. A distance restraint was applied to the O2-H2 bond. For **4**, H2 was introduced from its difference map position and allowed to refine isotropically and for position. All other hydrogen atoms were introduced in calculated positions and refined on a riding model. All non-hydrogen atoms were refined anisotropically. For **3**·THF, one half-occupancy, disordered THF molecule is present about a two-fold screw axis (the symmetry operation must be applied to generate the full molecule.) Similarity restraints were applied to atoms in that molecule. H-atoms for the disordered THF could not be located from difference maps, and could not be satisfactorily introduced by calculation into ideal geometries, and were therefore omitted from the model. They have been included in the formula for the calculation of intensive properties. There is an intramolecular π-π interaction between one of the phenolate rings and the pyridyl pendant within one molecule. Plane to plane angle: 28.04(9)°. Plane centroid to plane centroid distance: 3.6709(19) Å. Plane to plane shift distance: 0.424(4) Å. There is intermolecular π-π interaction between two molecules which are not bonded via hydrogen bonding, that is between the hydrogen bonded dimers. One pyridyl group of such a dimer exhibits π-π interaction with another pyridyl group of another dimer. Plane to plane angle: 4.87(14)°. Plane centroid to plane centroid distance: 3.634(3) Å. Plane to plane shift distance: 0.417(5) Å.

The higher R value for **4** is due to the poorly diffracting nature of the crystals coupled with their small size. Although a lower R value can be achieved by removing data above 2θ of 25°, the decrease of the data:parameter ratio coupled with the use of primarily low-angle data makes this a nonviable solution. Furthermore, since the connectivity is the primary purpose of the structure (i.e., the bond lengths and angles are typical of lithium phenolate complexes), we opted for the standard approach of using the complete data set.

References:

1. Dolomanov, O.V., Bourhis, L.J., Gildea, R.J, Howard, J.A.K. & Puschmann, H. (2009), J. Appl. Cryst. 42, 339-341.
2. Sheldrick, G.M. (2015). Acta Cryst. A71, 3-8.
3. Sheldrick, G.M. (2008). Acta Cryst. A64, 112-122.

Table S1. Crystallographic and structure refinement data for **3**·THF and **4**.

Compound	**3·THF**	**4**
Chemical formula	$C_{30}H_{39}N_2NaO_4\cdot1.5(C_4H_8O)$	$C_{30}H_{39}LiN_2O_4\cdot(C_7H_8)$
Colour	Colourless	Colourless
Habit	Prism	Prism
Crystal dimensions [mm]	0.36 × 0.31 × 0.24	0.20 × 0.20 × 0.20
Formula weight	622.80	590.71
Crystal system	Monoclinic	Monoclinic
a [Å]	22.745(7)	17.399(7)
b [Å]	16.871(5)	12.202(5)
c [Å]	18.568(6)	19.503(10)
α [°]	90	90
β [°]	104.513(4)	127.700(9)
γ [°]	90	90
Unit cell V [Å^3]	6898(4)	3276(3)
Temperature [K]	123 ± 1	153 ± 2
Space group	C2/c (#15)	$P2_1/c$ (#14)
Z	8	4
D_c/g cm^{-3}	1.199	1.198
Radiation type	MoKα	MoKα
μ (MoKα) [cm^{-1}]	0.90	0.76
F(000)	2688	1272
Reflections measured	21786	8557
Unique refl's	7065	4562
R_{int}	0.0333	0.0904
R_1 (all)	0.0905	0.2006
$wR(F_2)$ (all)	0.2275	0.2396
R_1 ($I > 2\sigma(I)$)[a]	0.0789	0.1163
$wR(F^2)$ ($I > 2\sigma(I)$) [b]	0.2156	0.1988
Goodness of fit on F^2	1.091	1.082
CCDC Ref.	1535025	1535026

[a] $R_1 = \Sigma(|F_o| - |F_c|)/\Sigma|F_o|$; $wR_2 = [\Sigma(w(F_o^2 - F_c^2)^2)/\Sigma w(F_o^2)^2]^{1/2}$.

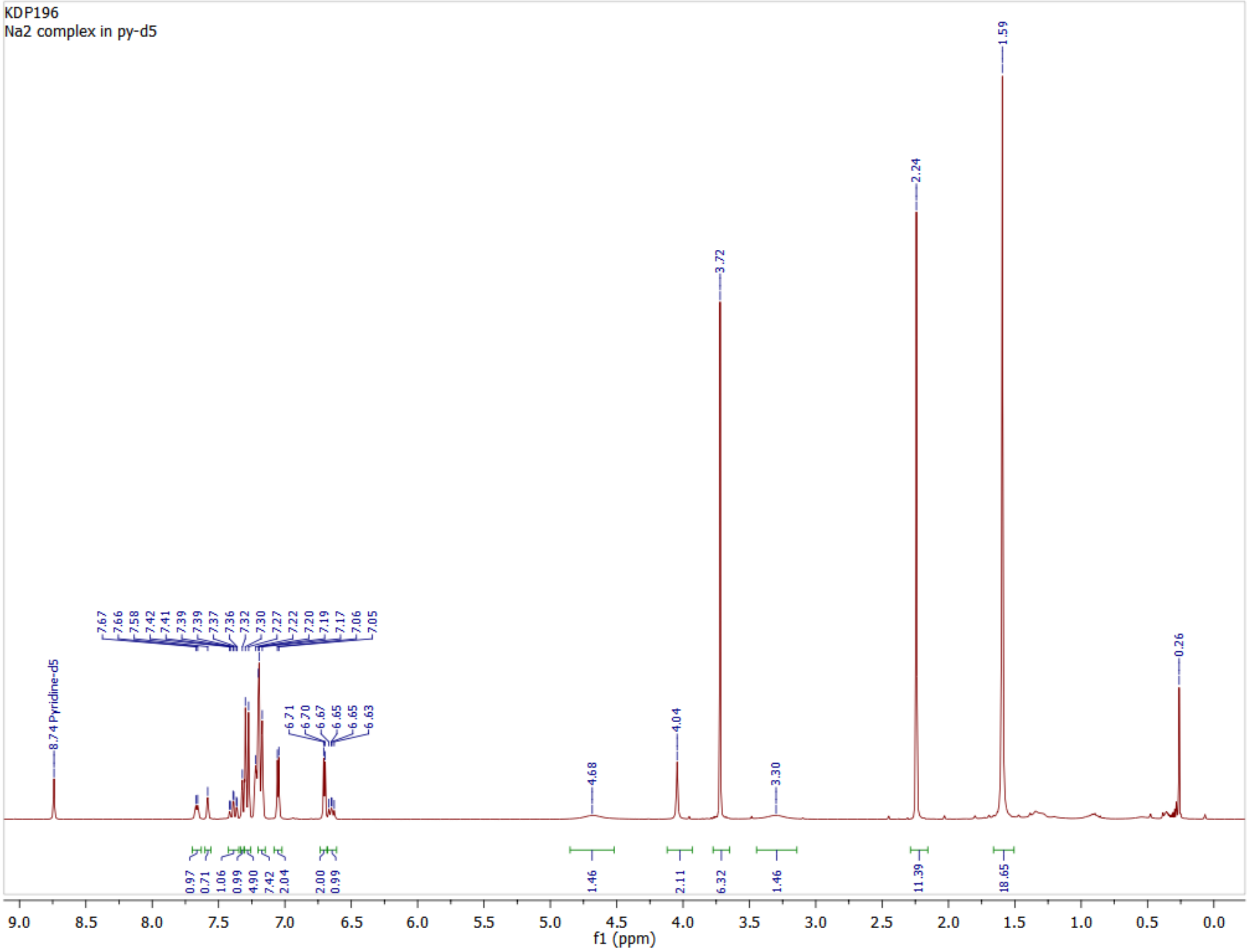

Figure S1. ^{1}H NMR spectrum of **1** in py-d_5 (prepared in toluene).

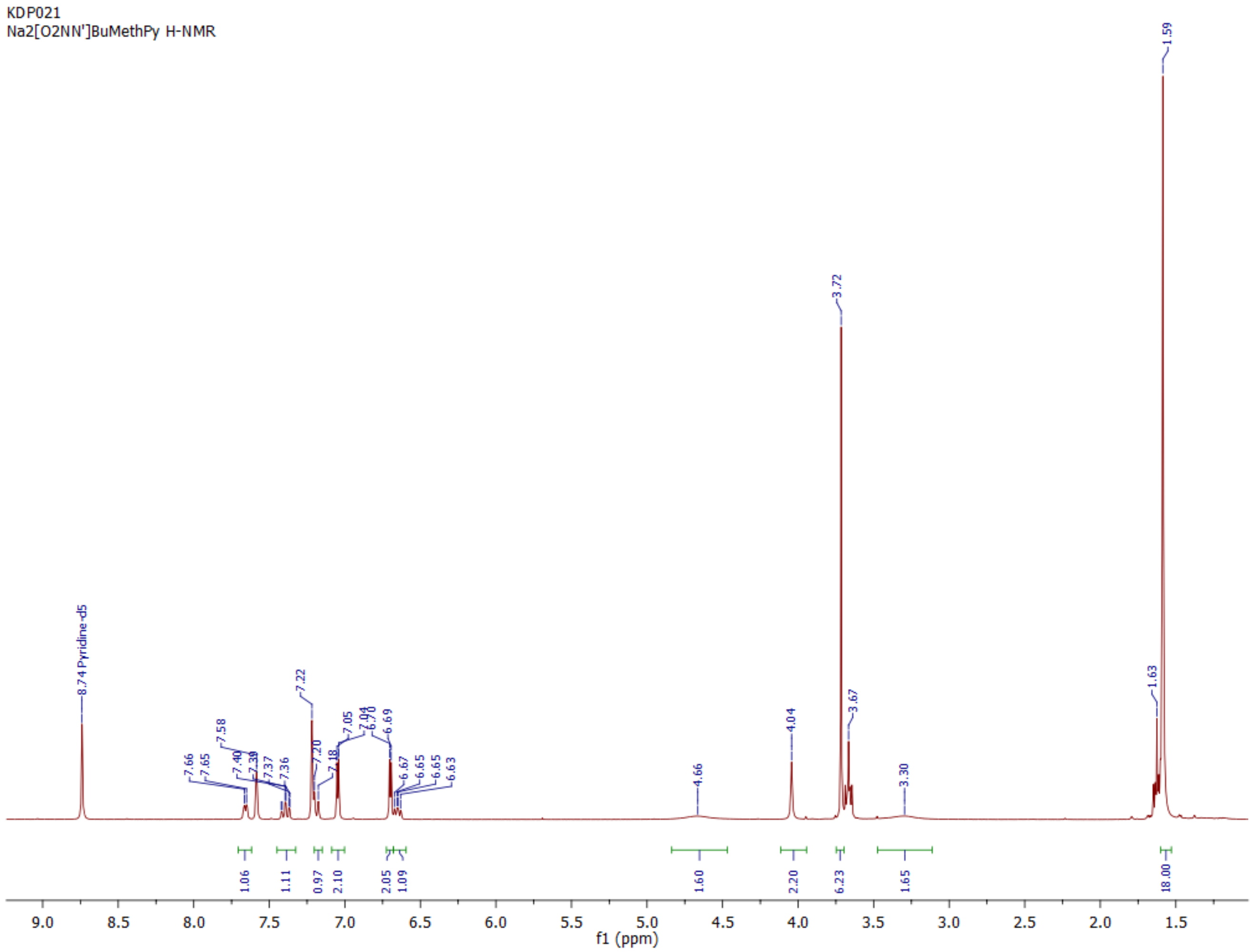

Figure S2. ^{1}H NMR spectrum of **1**·THF in py-d_5 (prepared in THF).

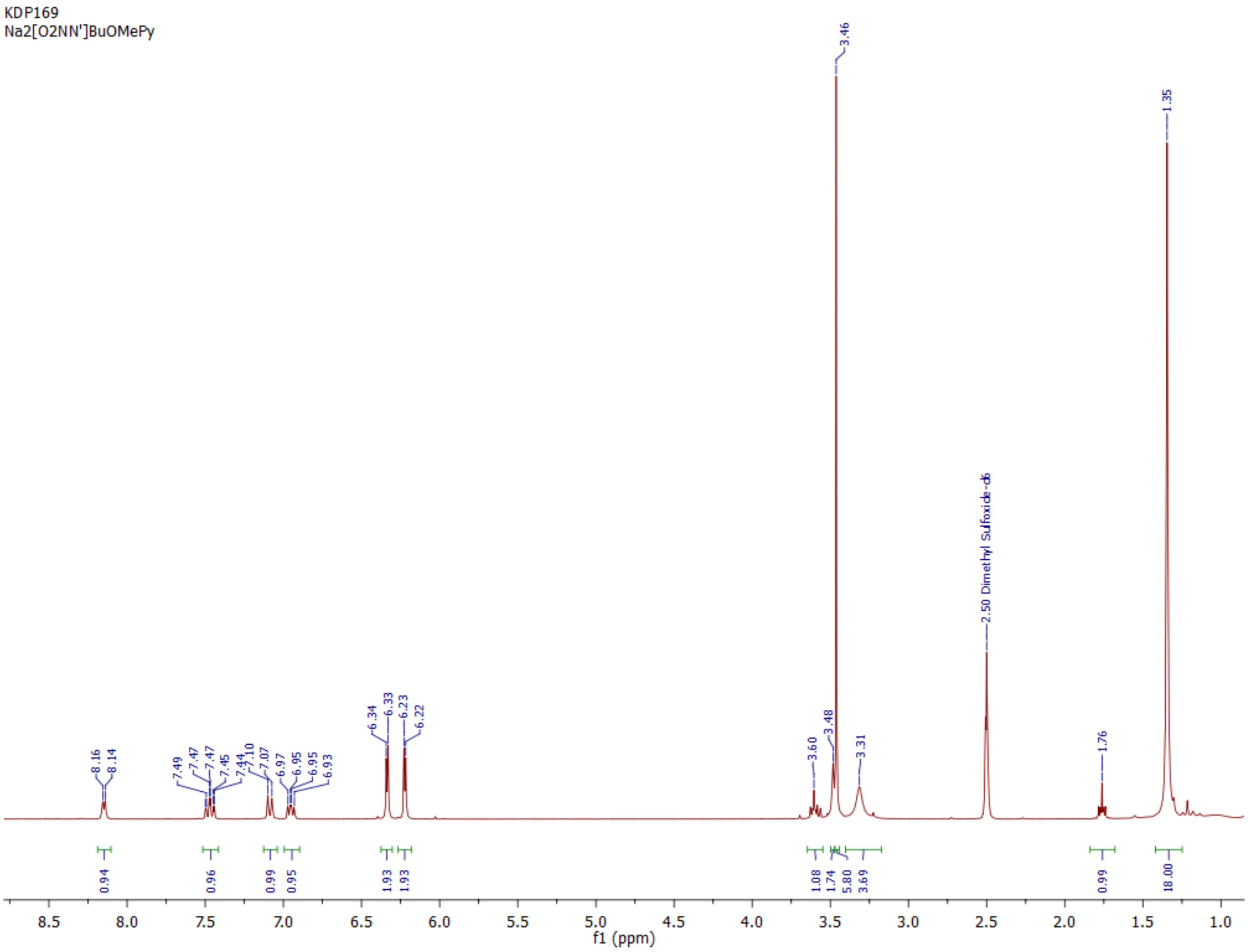

Figure S3. ^{1}H NMR spectrum of **1**·THF in DMSO-d$_6$ (prepared in THF).

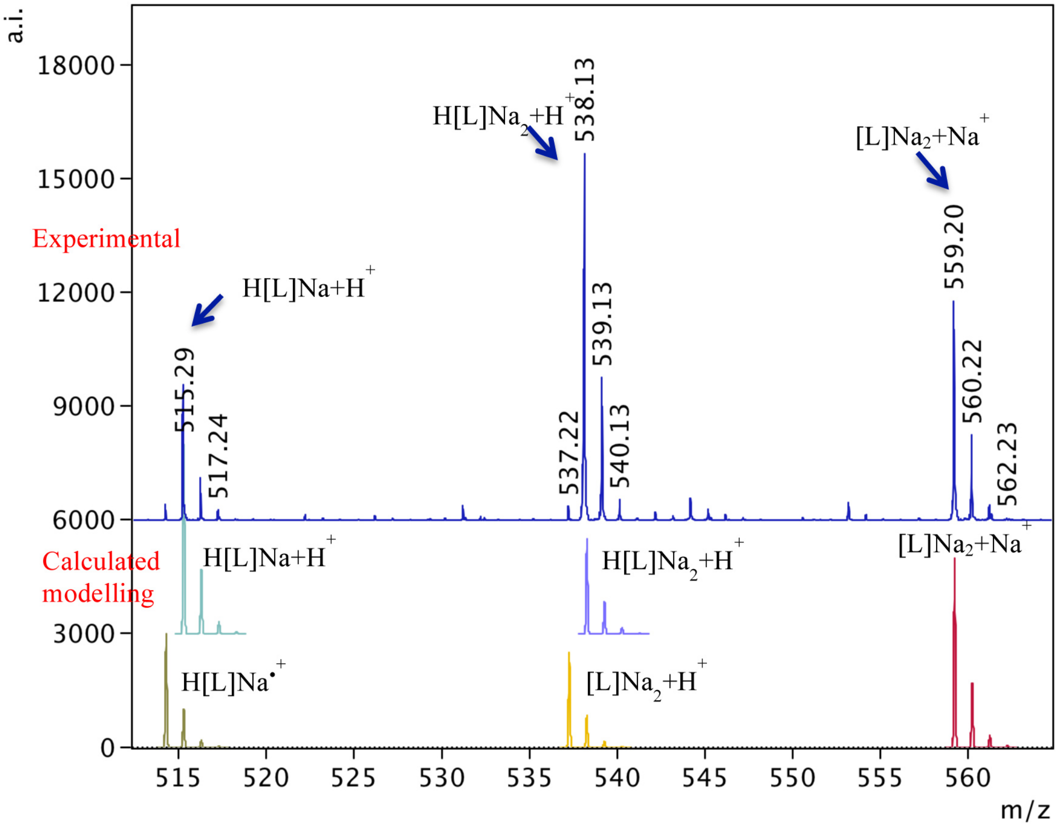

Figure S4. MALDI-TOF mass spectrum of **1**·THF with modeled calculated isotopic distribution patterns.

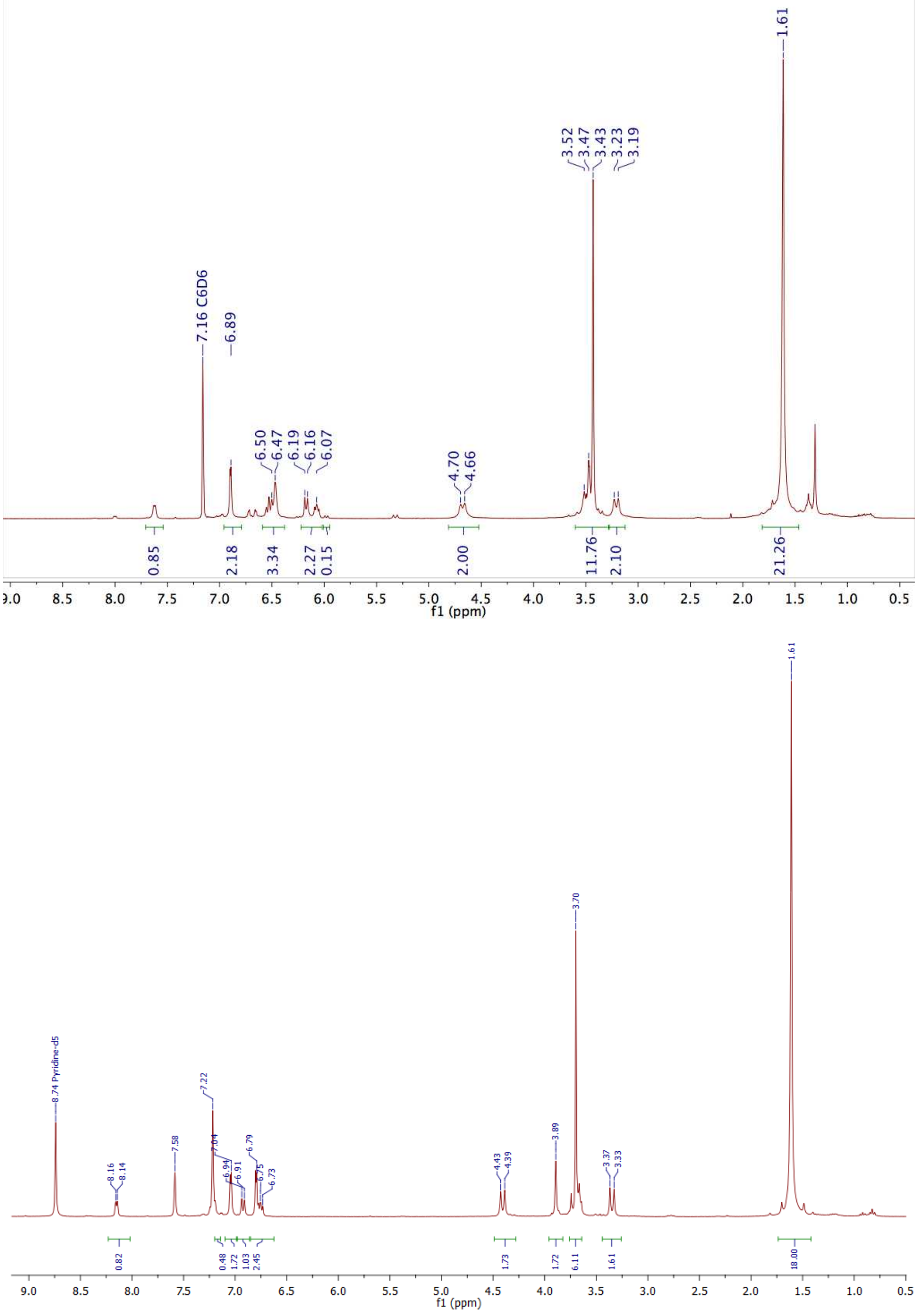

Figure S5. ^{1}H NMR spectrum of **2**·THF in C_6D_6 (top) and py-d_5 (bottom).

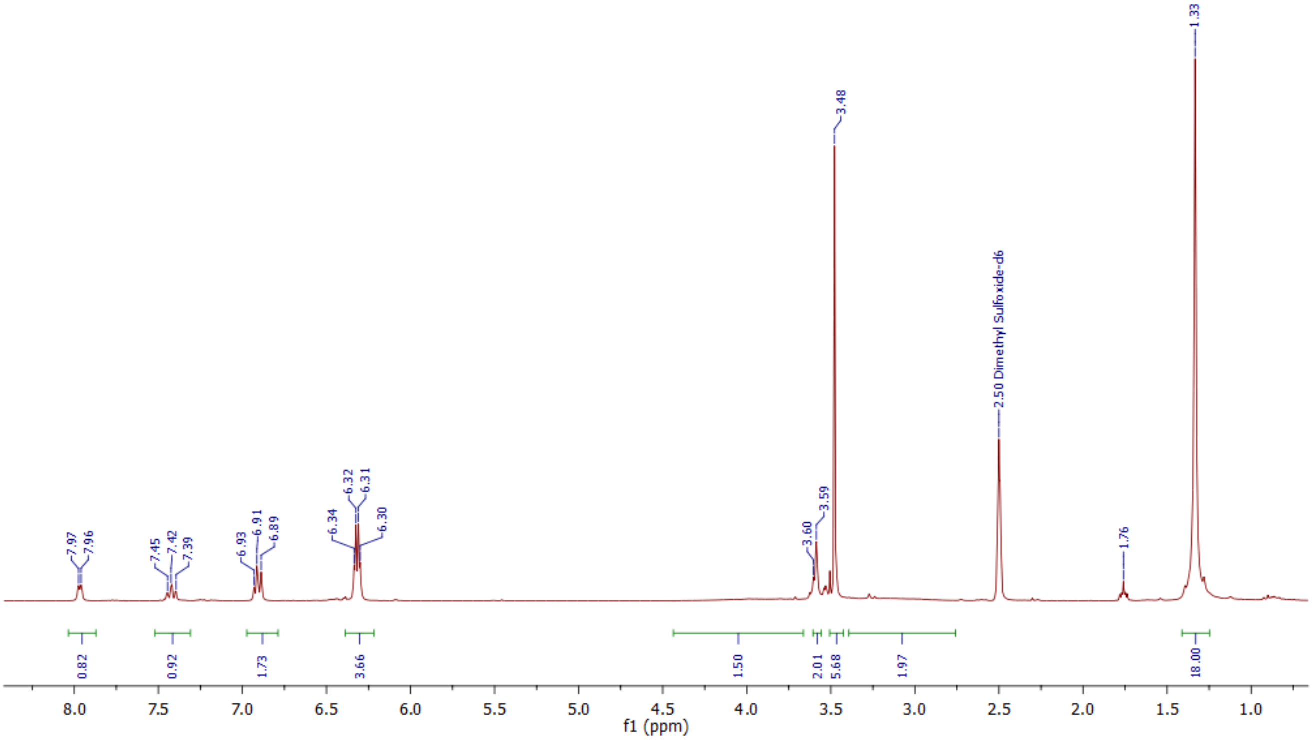

Figure S6. ^{1}H NMR spectrum of **2** in DMSO-d_6.

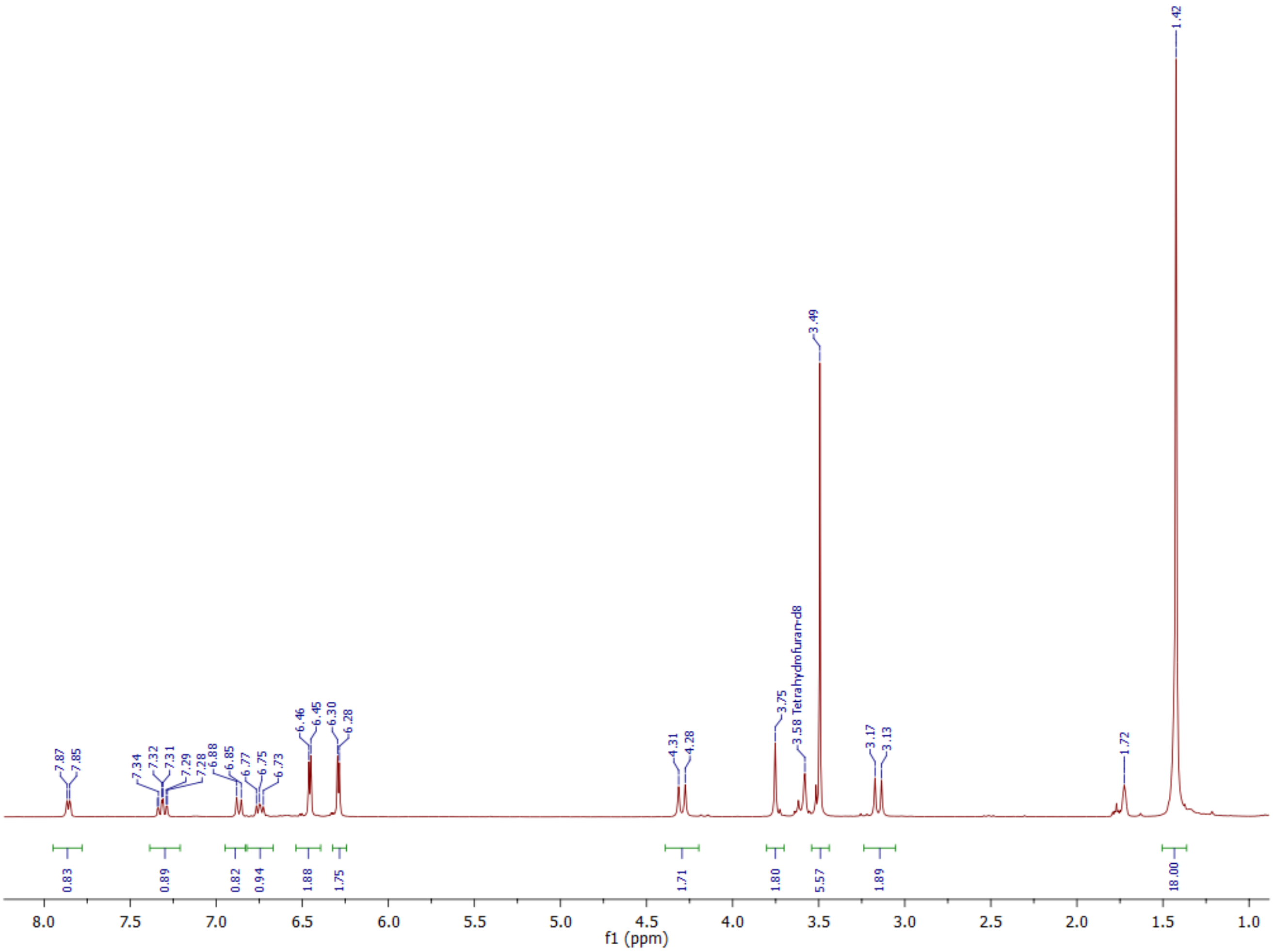

Figure S7. ^{1}H NMR spectrum of **2** in THF-d_8.

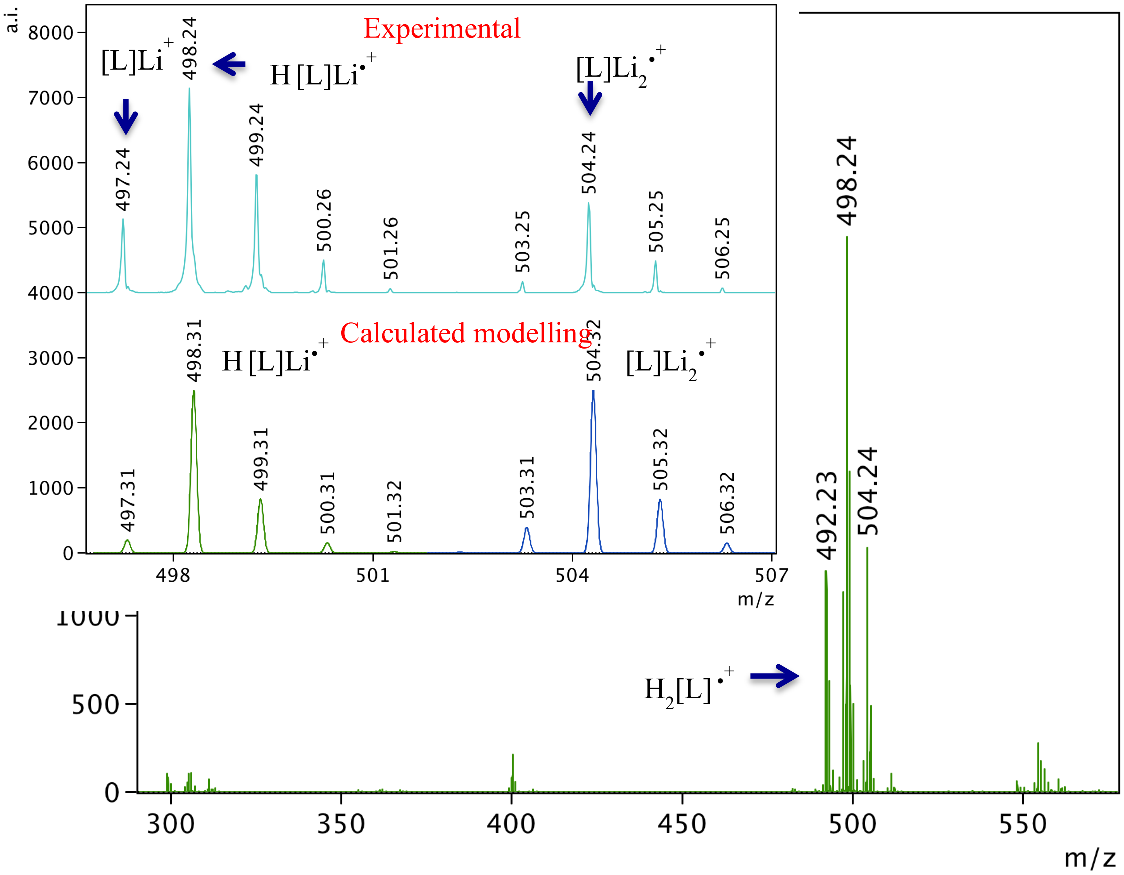

Figure S8. MALDI-TOF mass spectrum of **2**. Inset shows the comparison of the experimental and the modeled calculated isotopic distribution patterns.

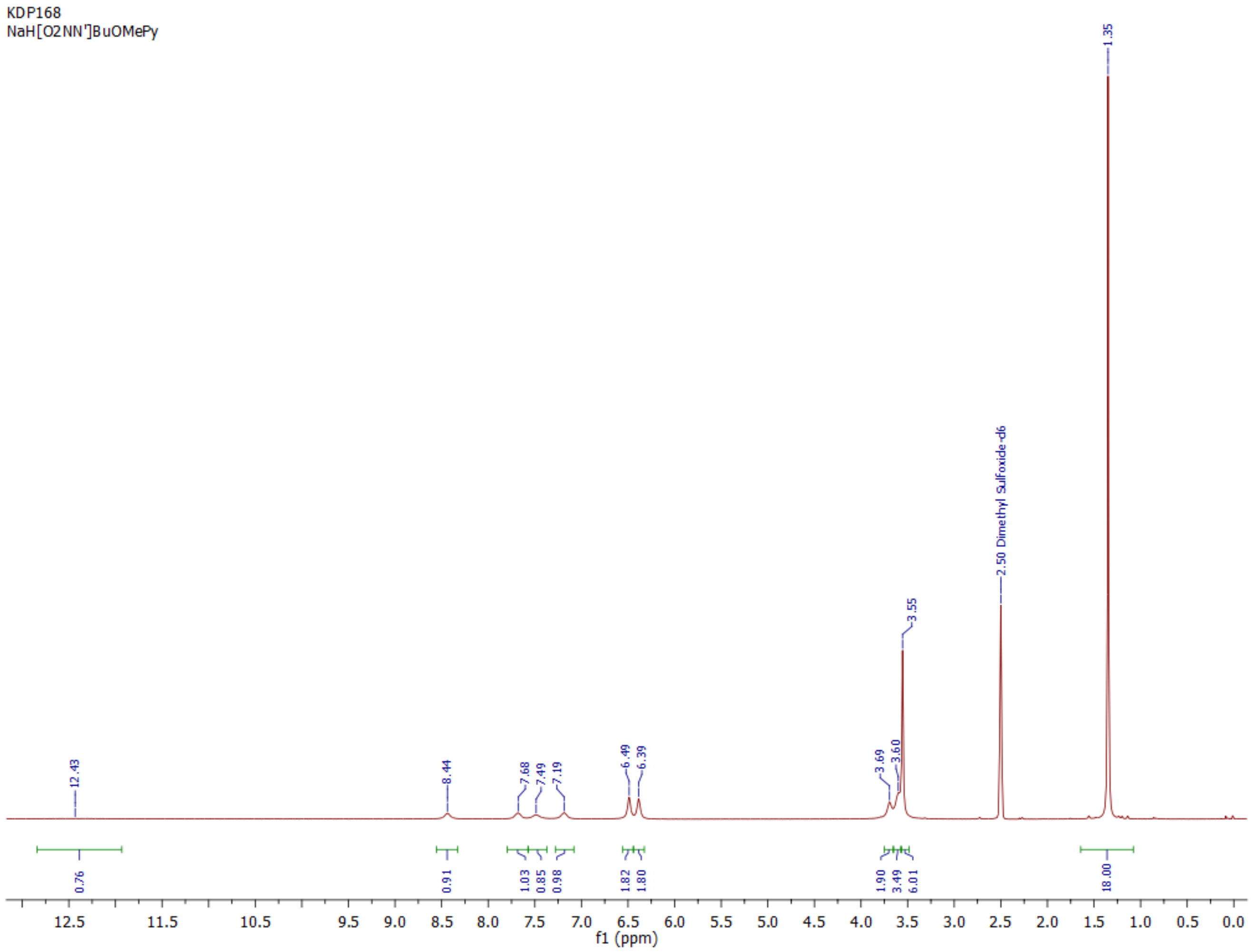

Fig. S9. ^{1}H NMR spectrum of **3** in DMSO-d_6.

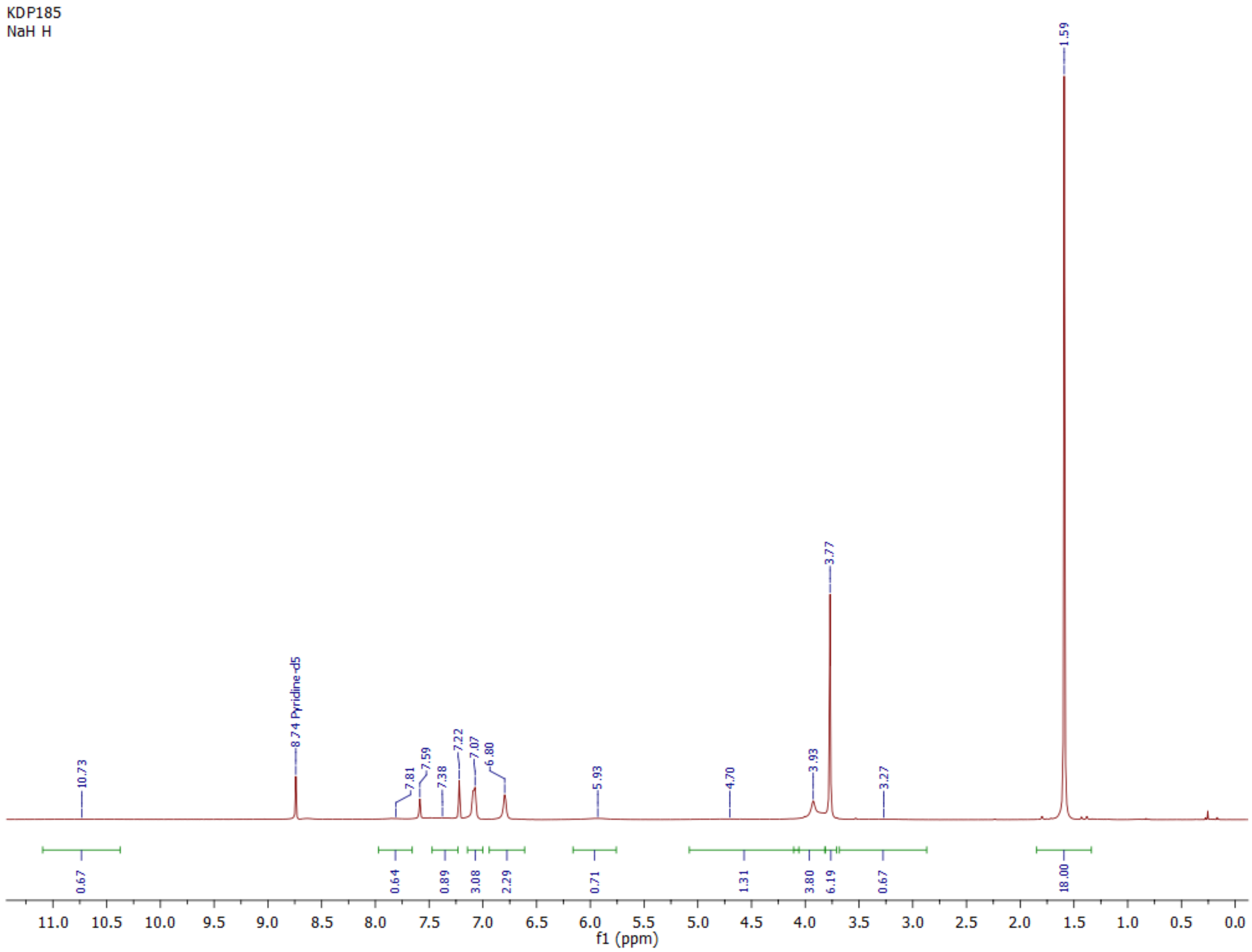

Fig. S10. ^{1}H NMR spectrum of **3** in py-d_5.

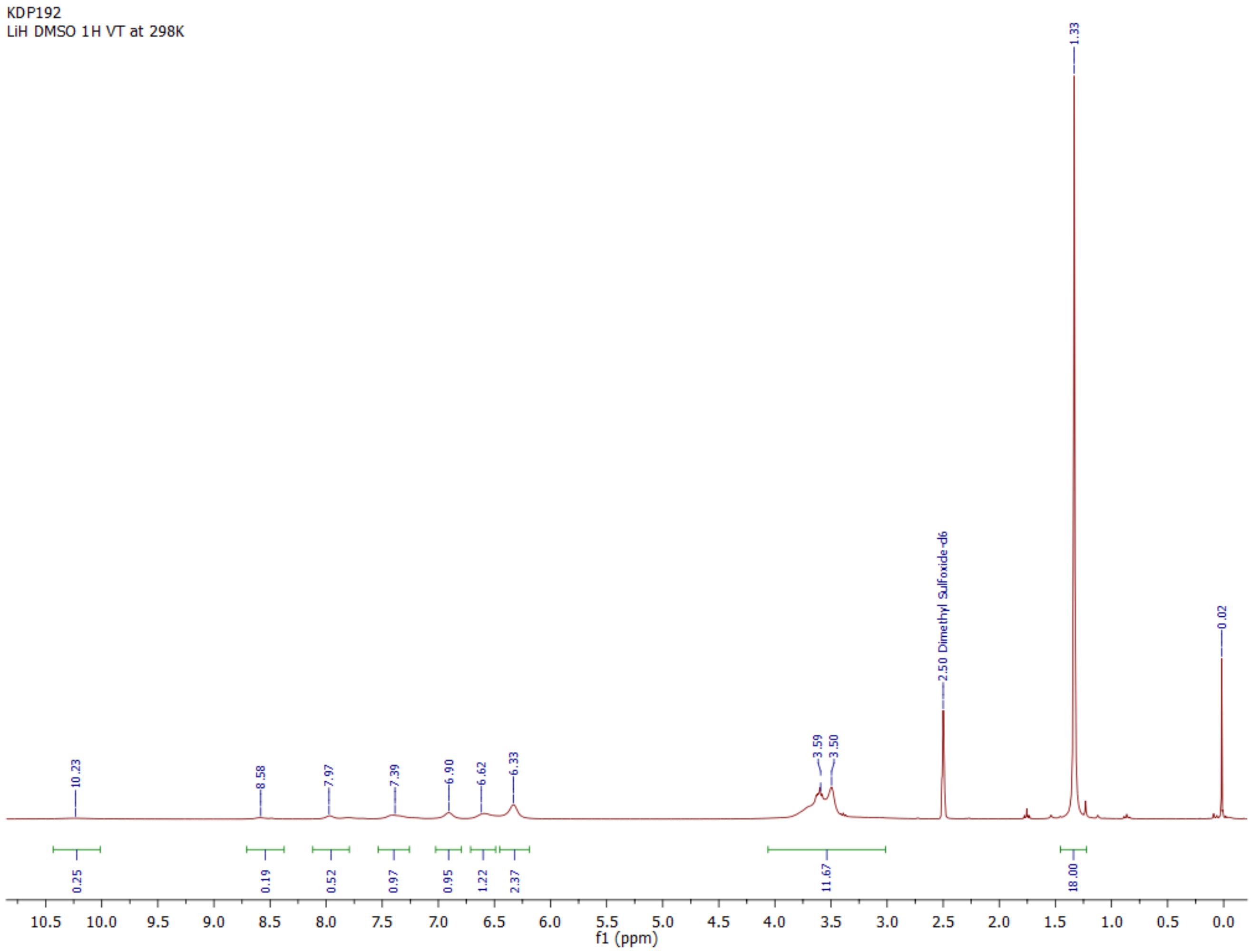

Fig. S11. ^{1}H NMR spectrum of **4** in DMSO-d$_6$.

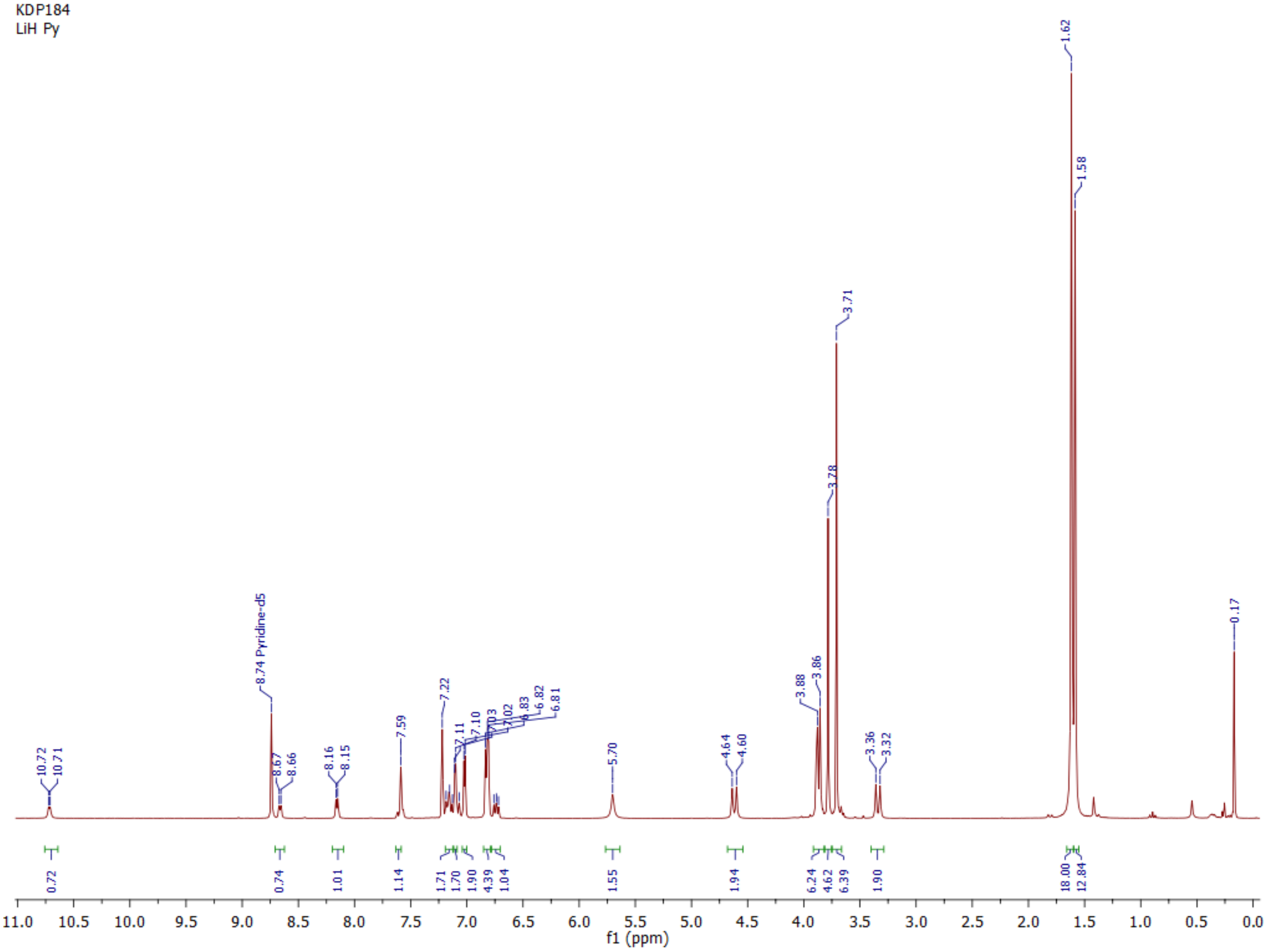

Fig. S12. ^{1}H NMR spectrum of **4** in py-d$_5$.

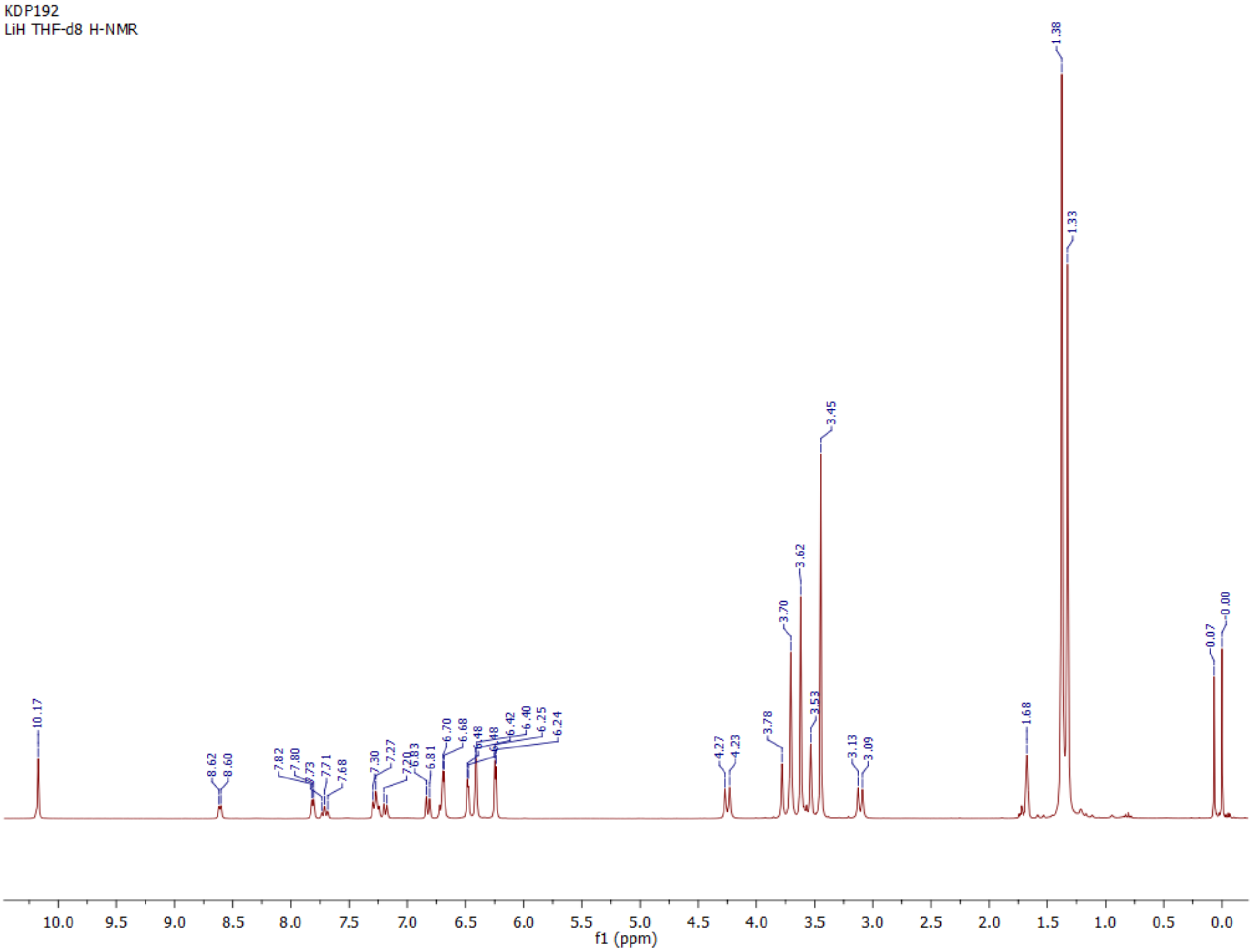

Fig. S13. ^{1}H NMR spectrum of **4** in THF-d_8.

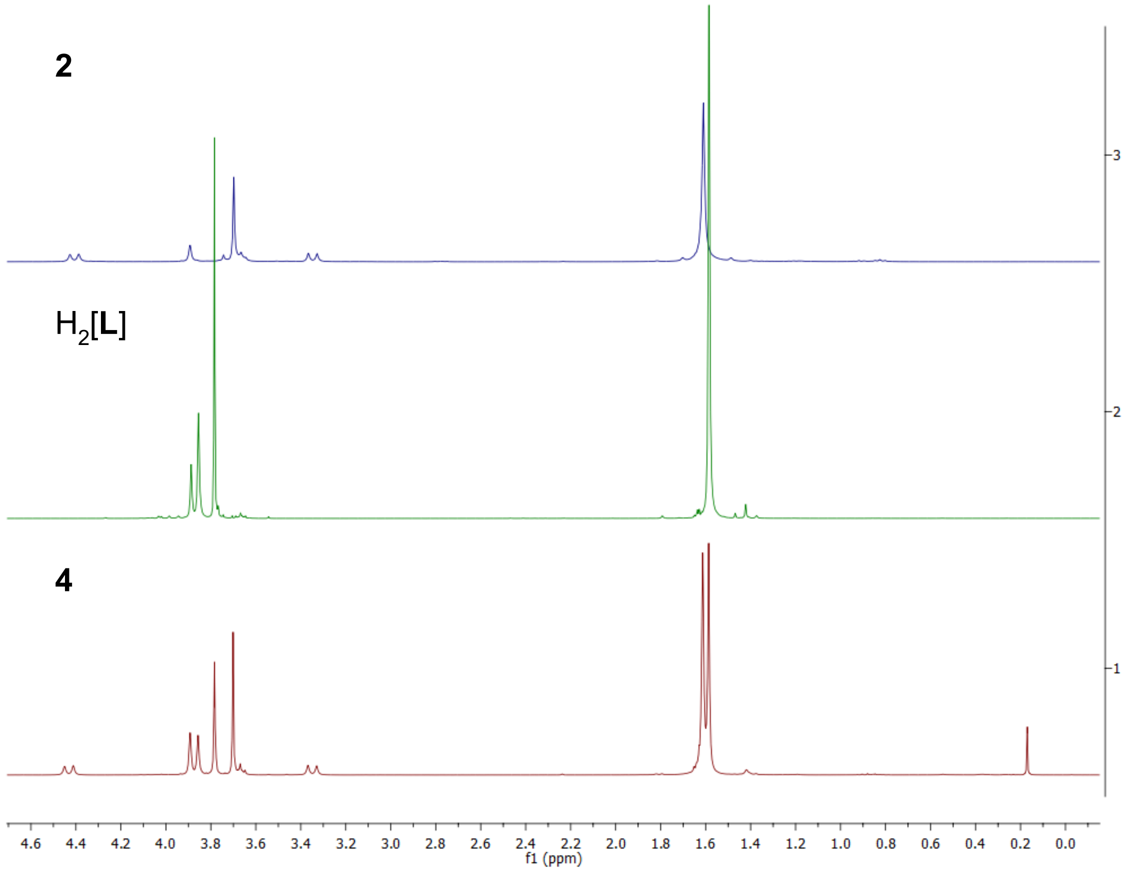

Figure S14. ^{1}H NMR spectra of **2,** H_2[**L**] and **4**, which results in a mixture of **2** and H_2[**L**] in py-d_5.

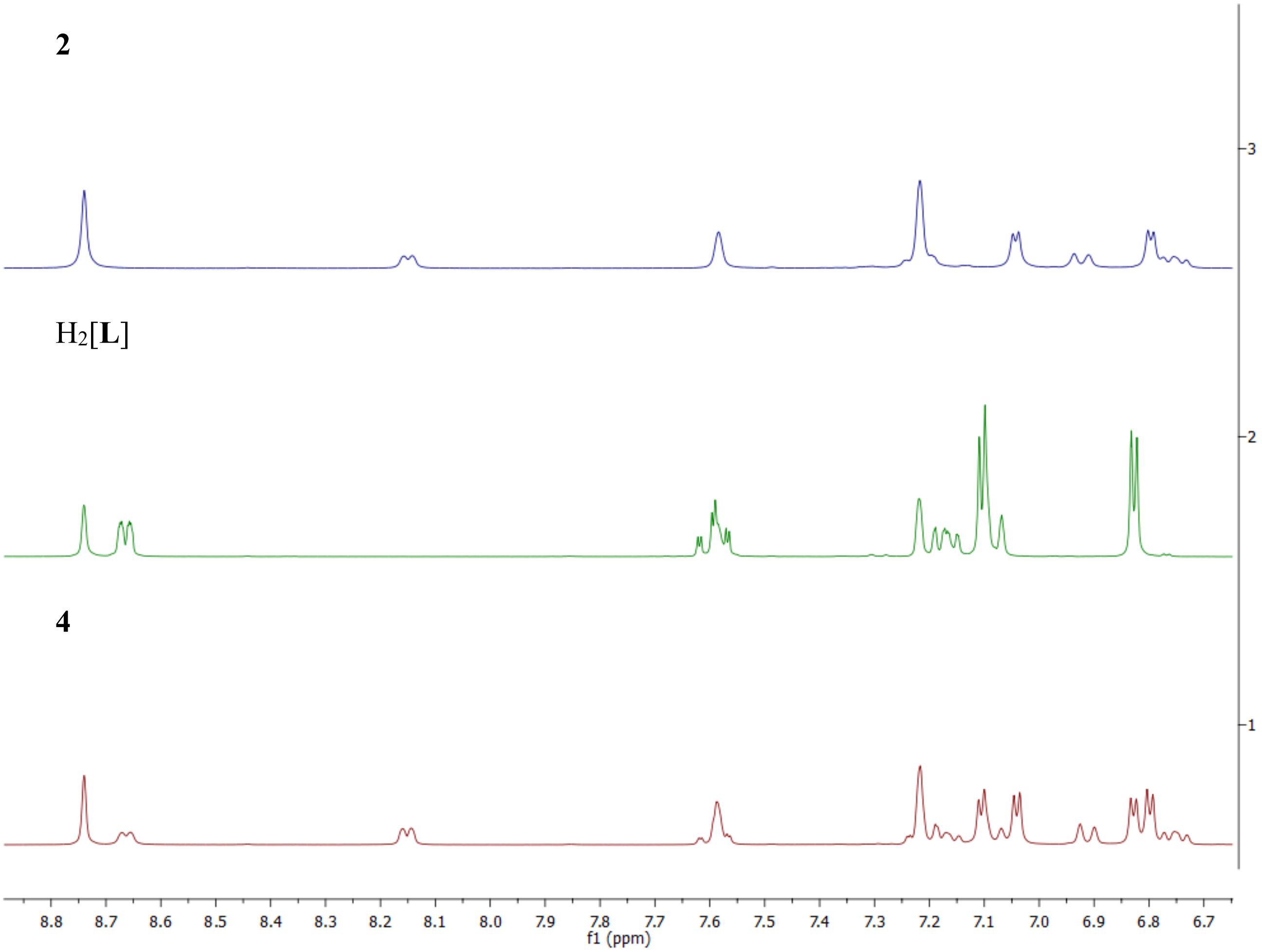

Figure S15. Aromatic region of the ^{1}H NMR spectra of complexes **2** and **4** and H_2[**L**]in py-d_5.

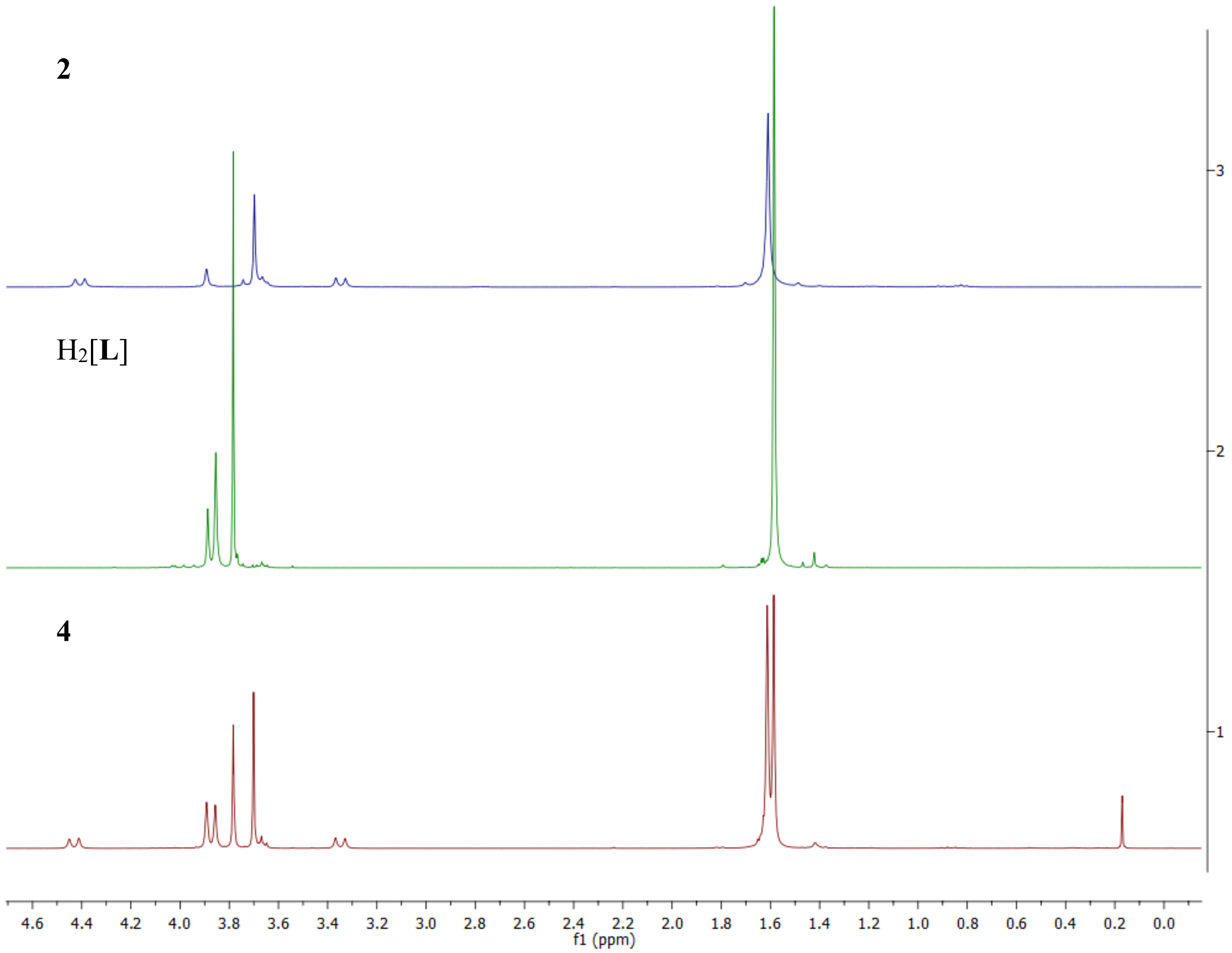

Figure S16. Methylene and methyl region of the ^{1}H NMR spectra of complexes **2** and **4** in py-d$_5$.

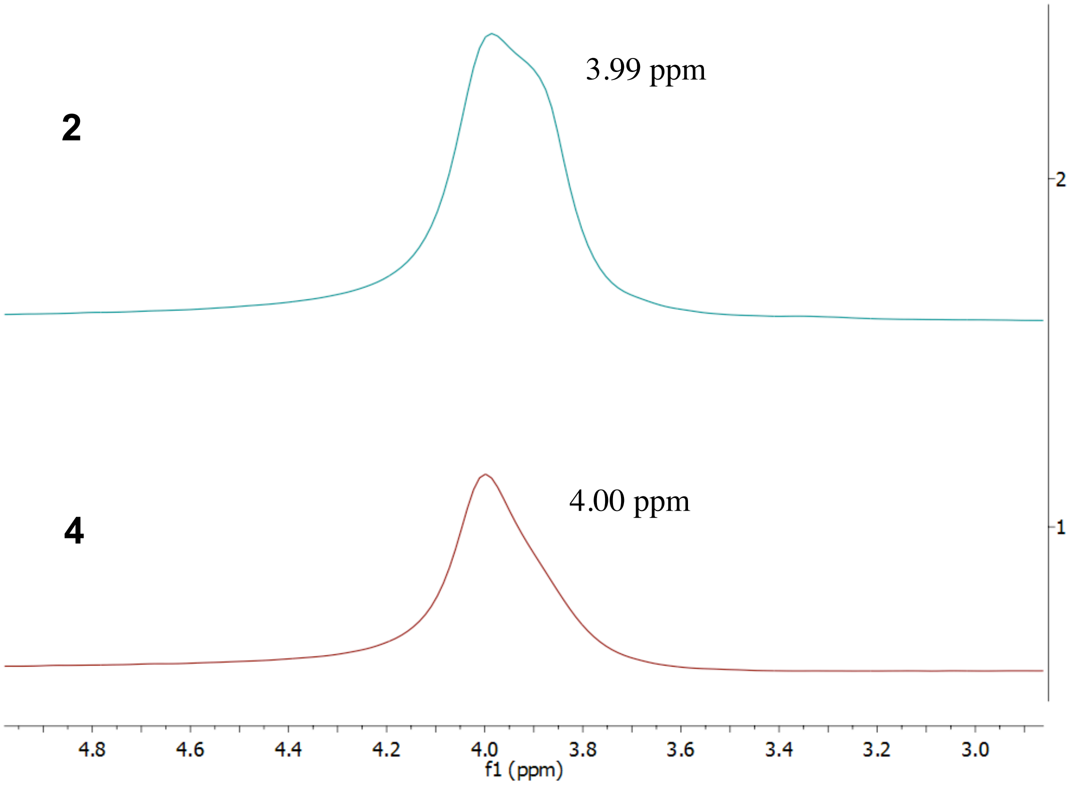

Figure S17. Stacked ^{7}Li NMR spectra of **2** and **4** in py-d_5 at a concentration of 0.1067 mol/L.

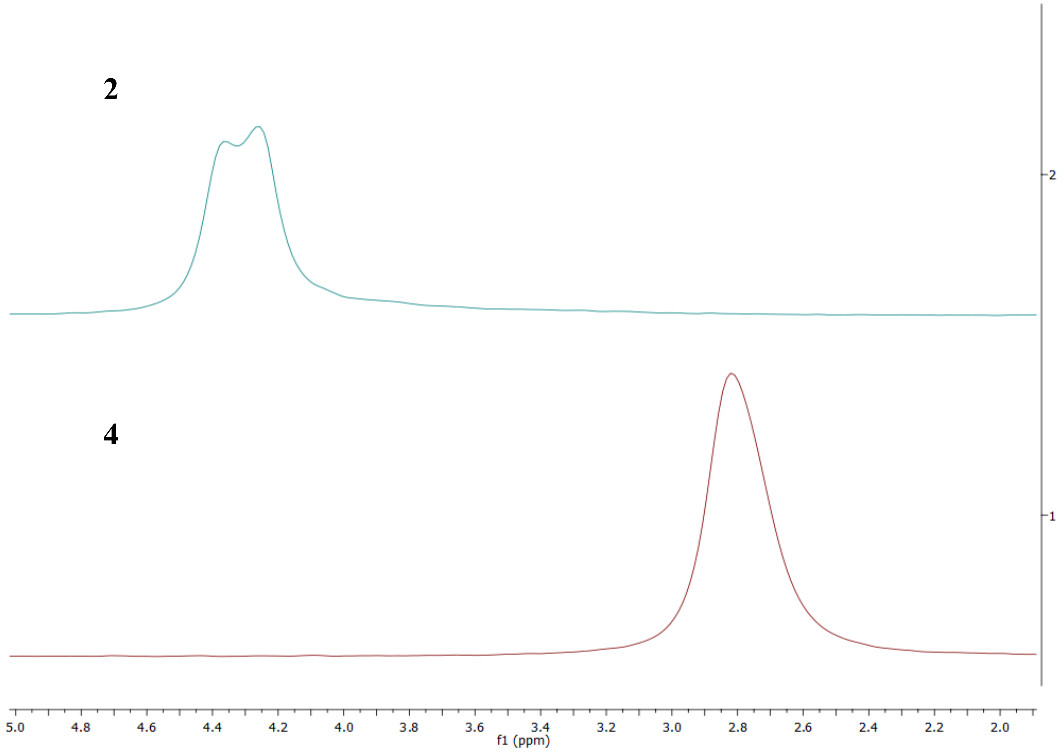

Figure S18. ^{7}Li NMR spectra of **2** and **4** in py-d_5 at a concentration of 0.0762 mol/L.

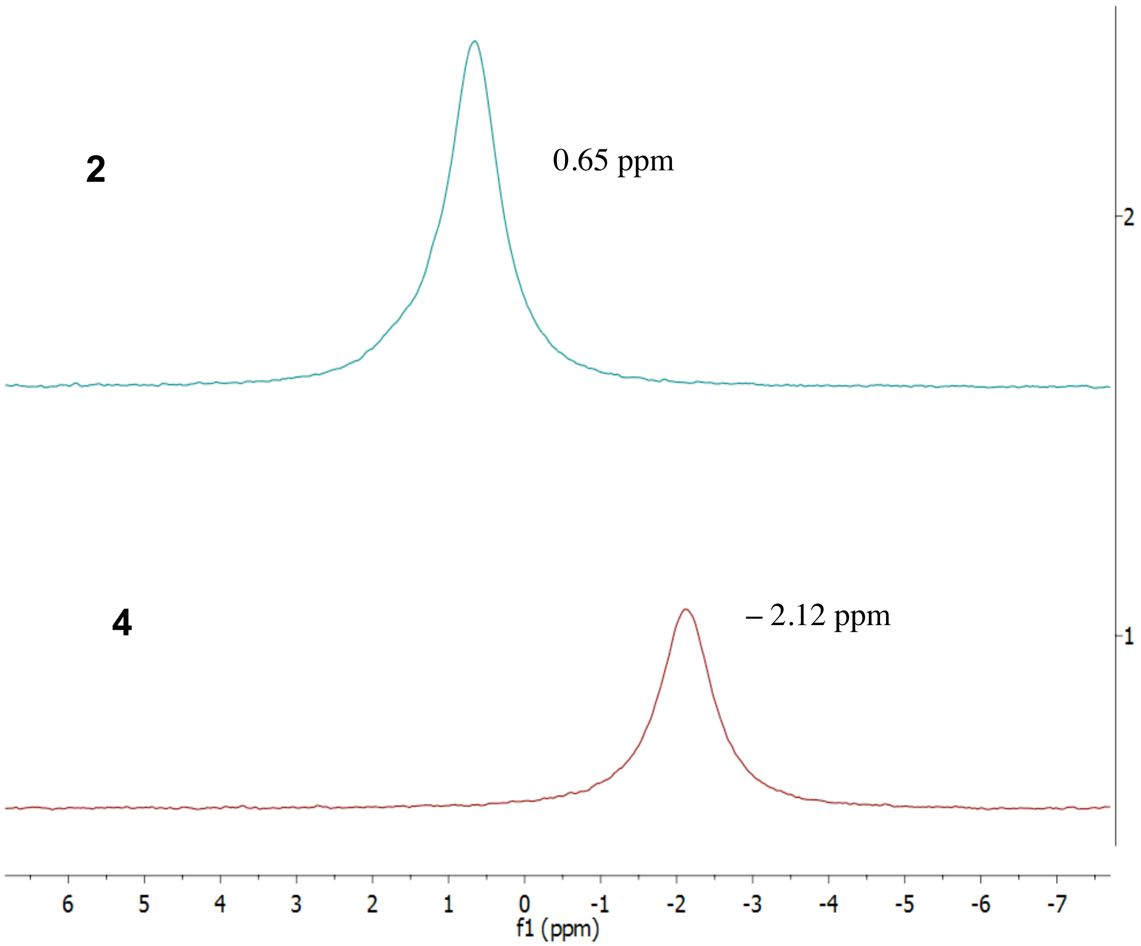

Figure S19. Stacked ^{7}Li NMR spectra of **2** and **4** in DMSO-d_6 at a concentration of 0.1067 mol/L.

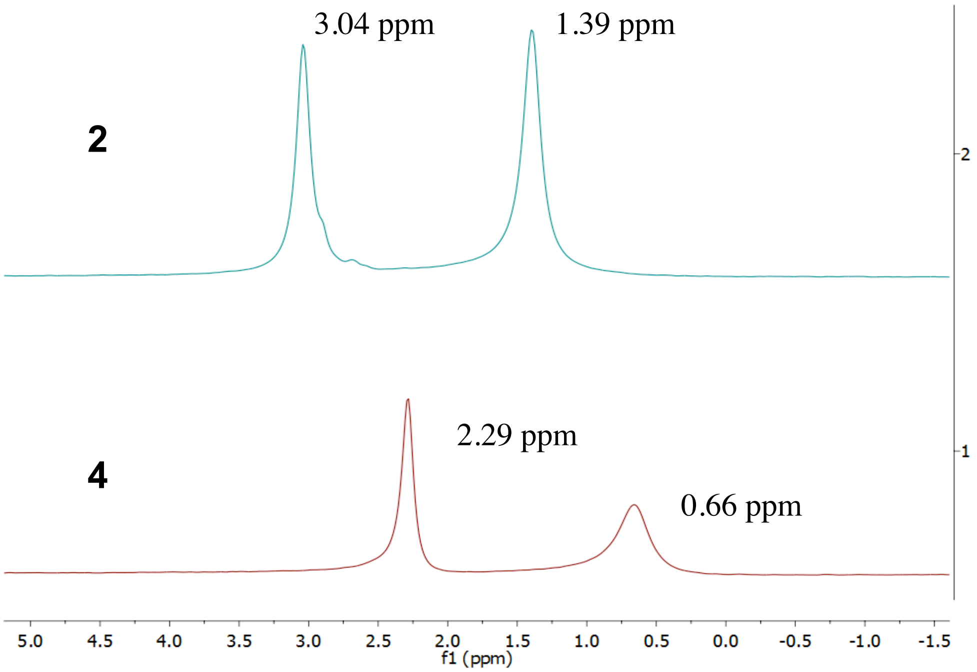

Figure S20. Stacked ^{7}Li NMR spectra of **2** and **4** at concentrations of 0.1067 mol/L in THF-d_8. In THF, **4** redistributes into a mixture of **2** and H_2[**L**].

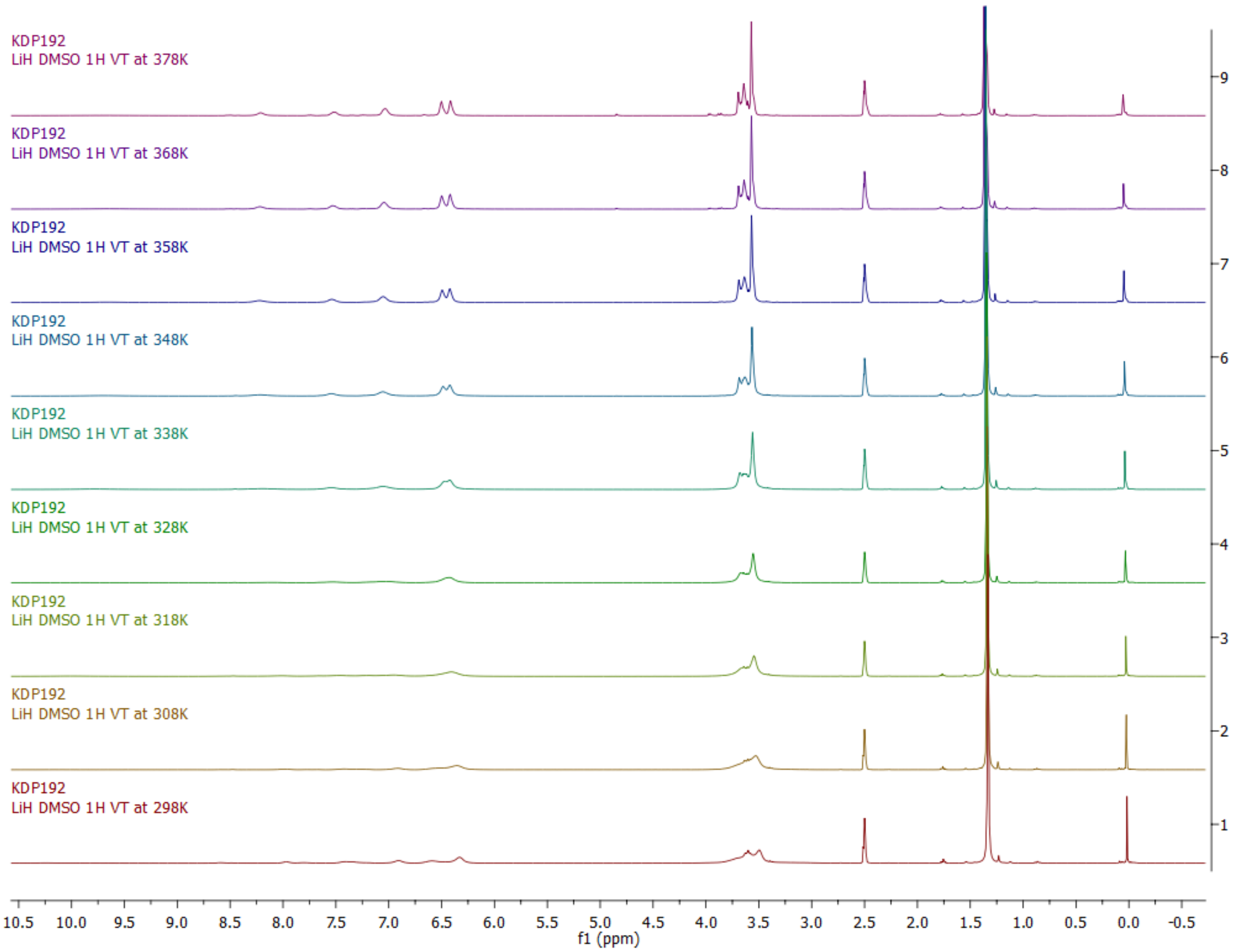

Figure S21. Variable temperature ^{1}H NMR spectra for **4** in DMSO-d$_6$.

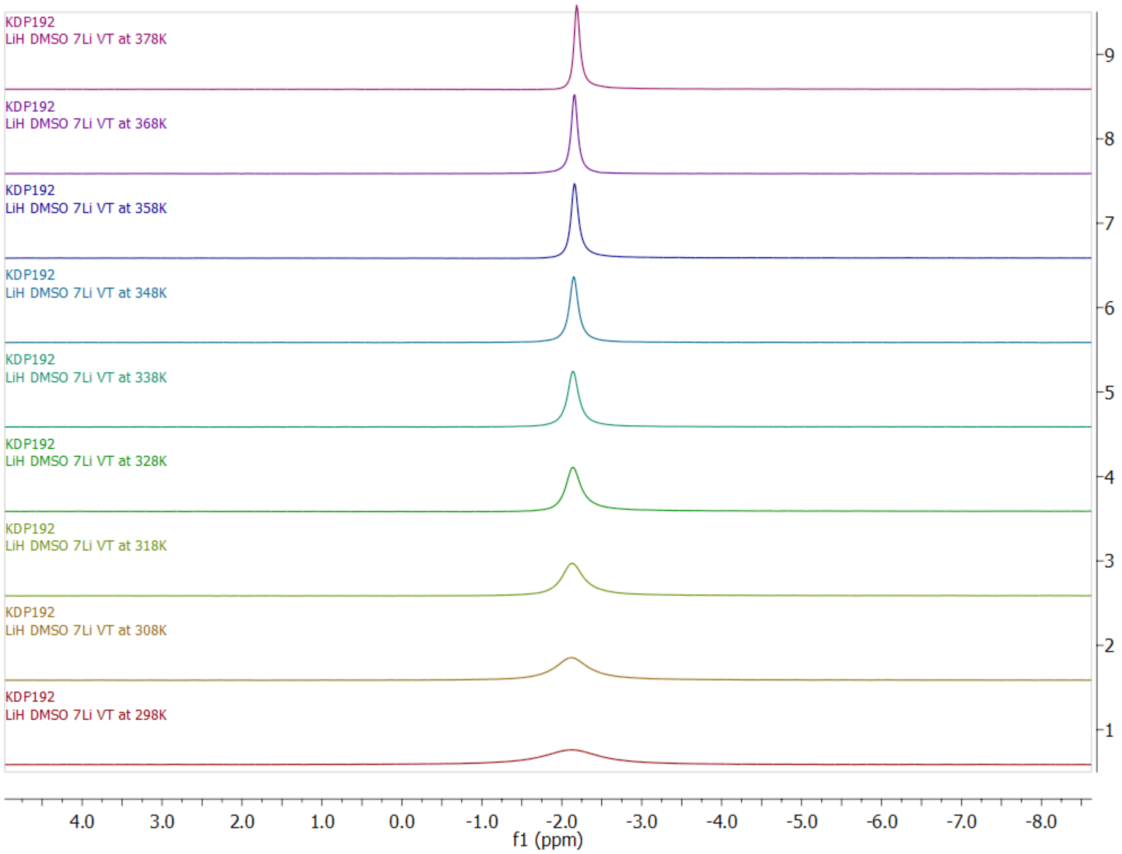

Figure S22. Variable temperature ^{7}Li NMR spectra for **4** in DMSO-d_6.

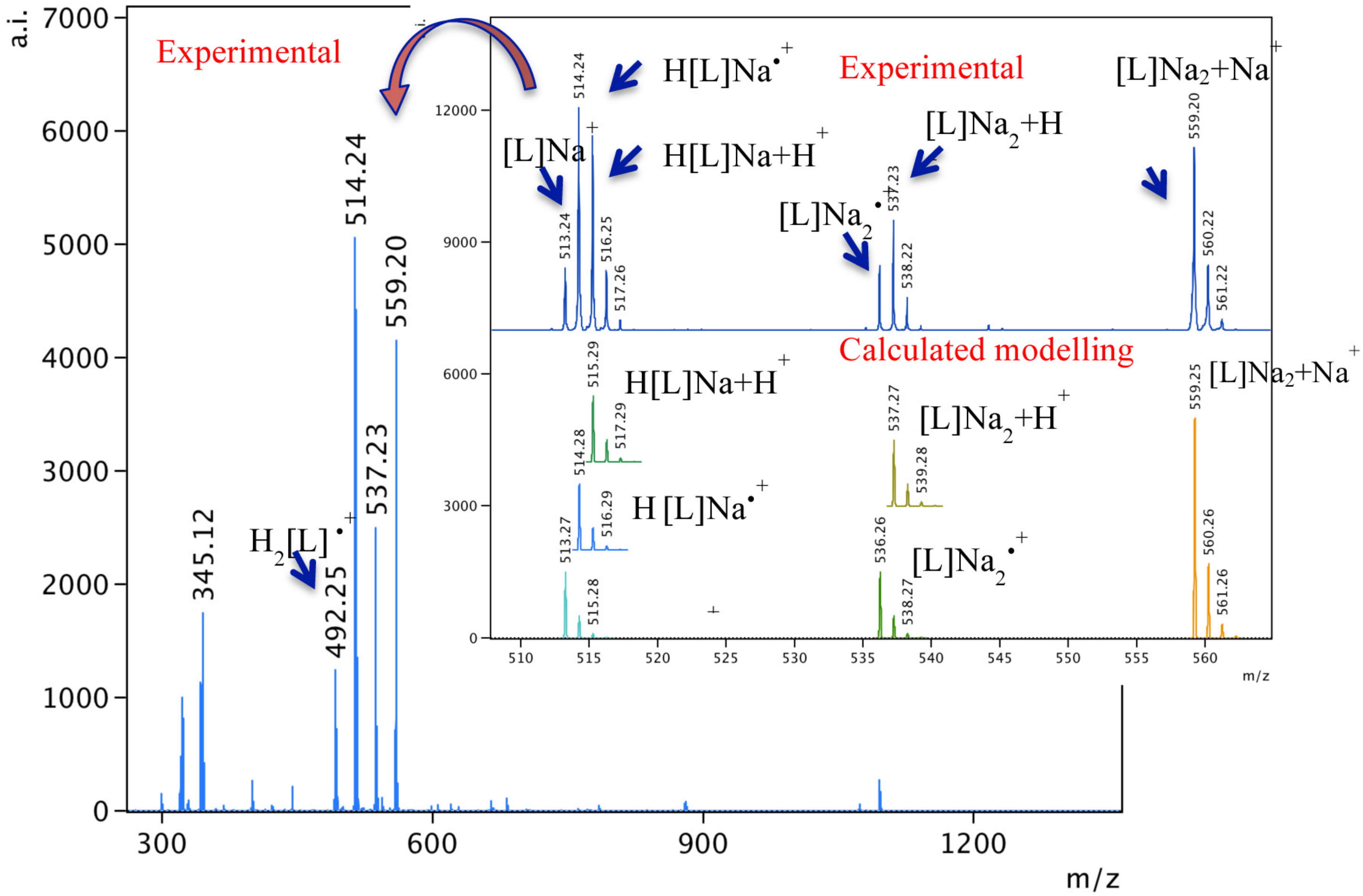

Figure S23. MALDI-TOF mass spectrum of **3**·THF. Inset: zoomed in region from *m/z* 510 – 565 and the calculated modeling of the isotopic distribution patterns of the peaks.

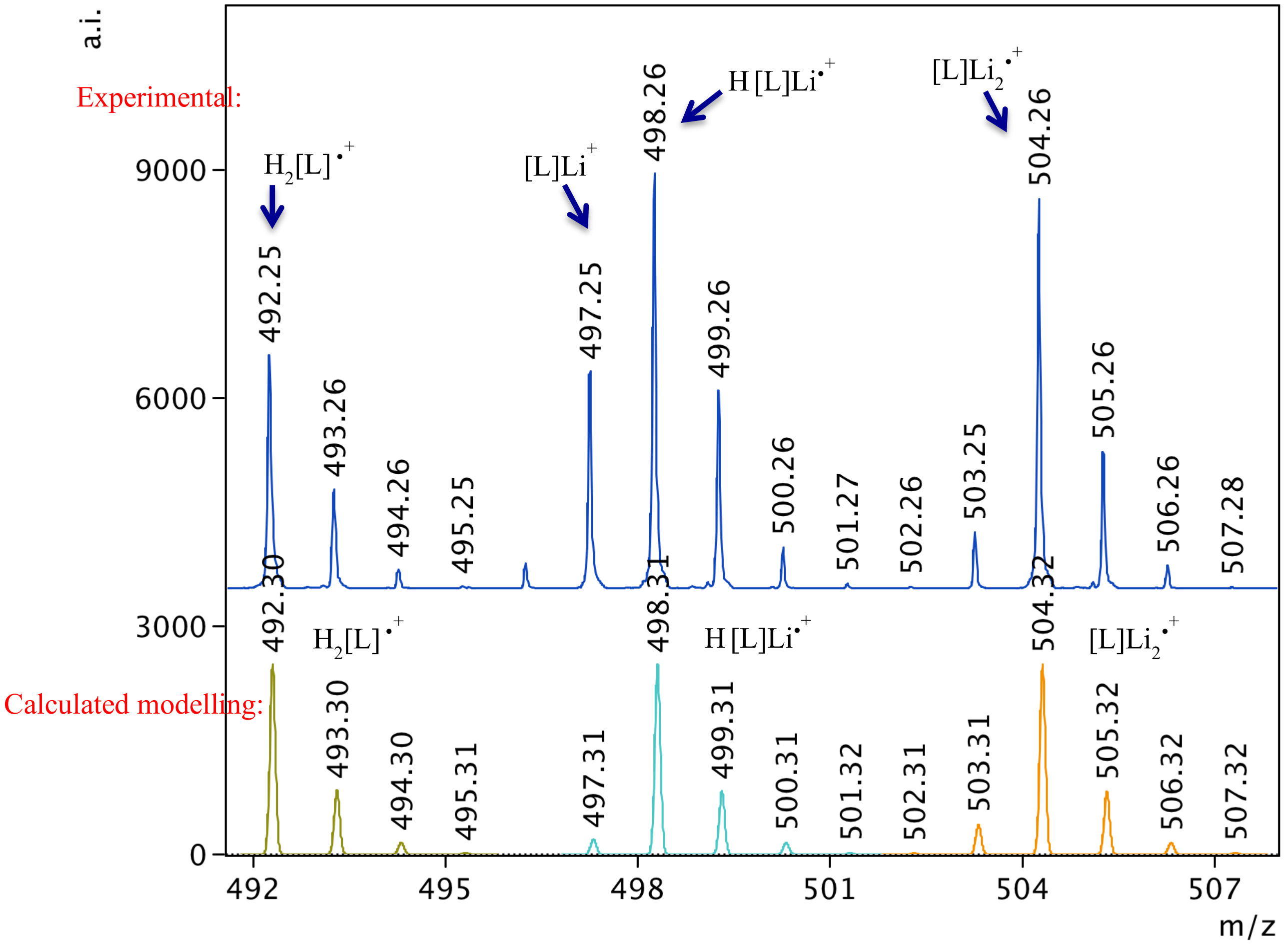

Figure S24. MALDI-TOF mass spectrum of **4** with calculated modeling isotopic distribution patterns.

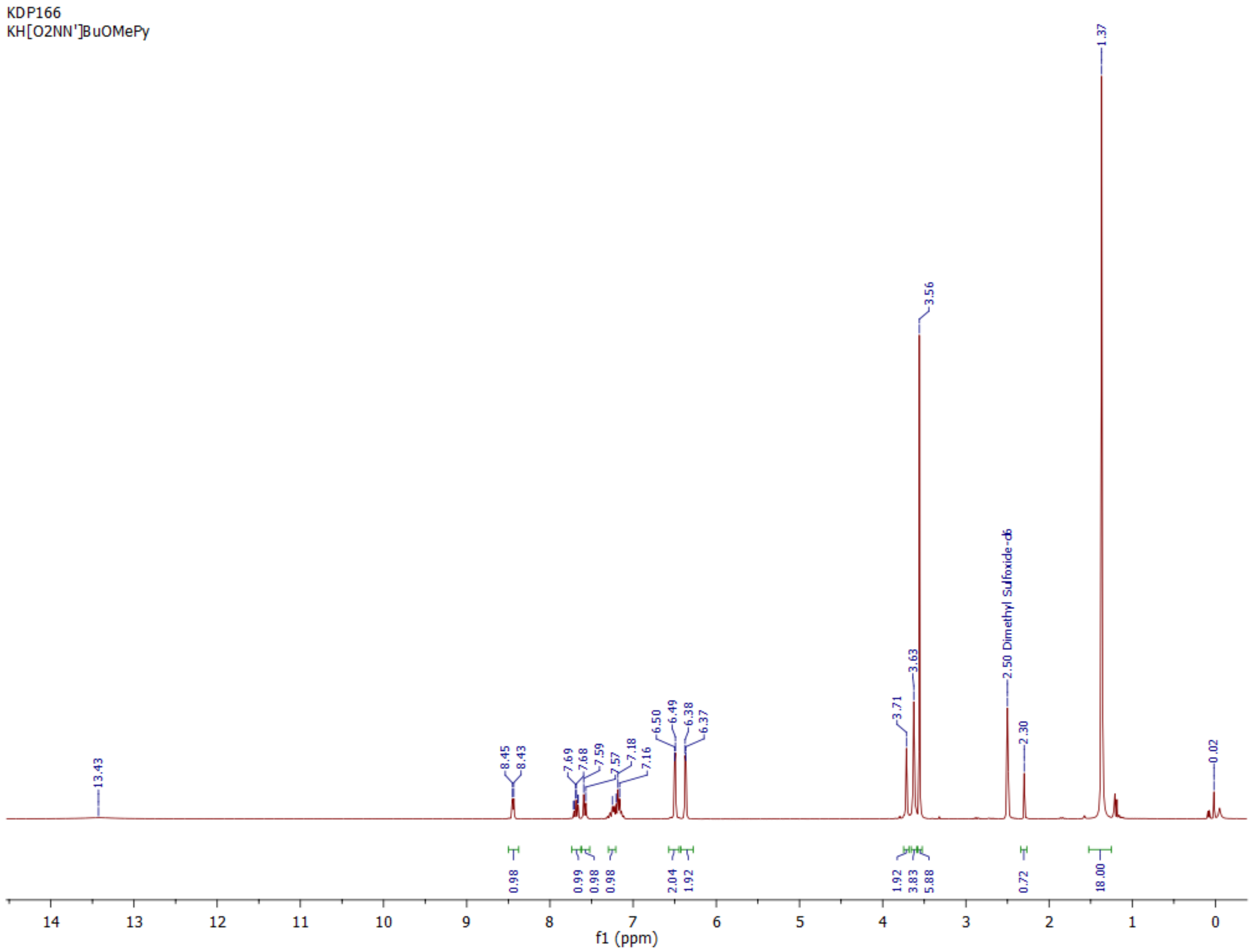

Fig. S25. ^{1}H NMR spectrum of **5** in DMSO-d$_6$.

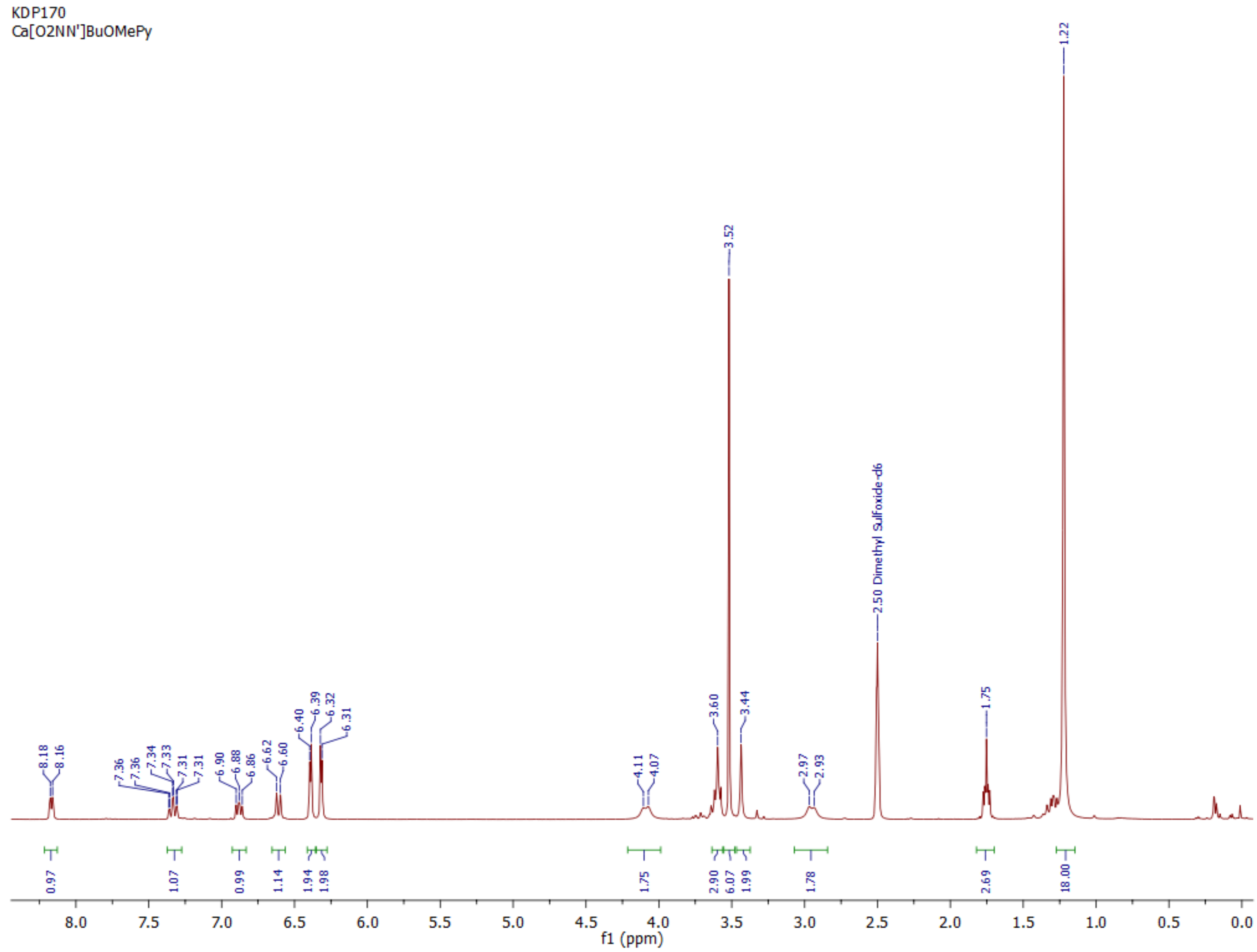

Figure S26. ^{1}H NMR spectrum of **6** in DMSO-d$_6$ prepared via route A) in Scheme 1.

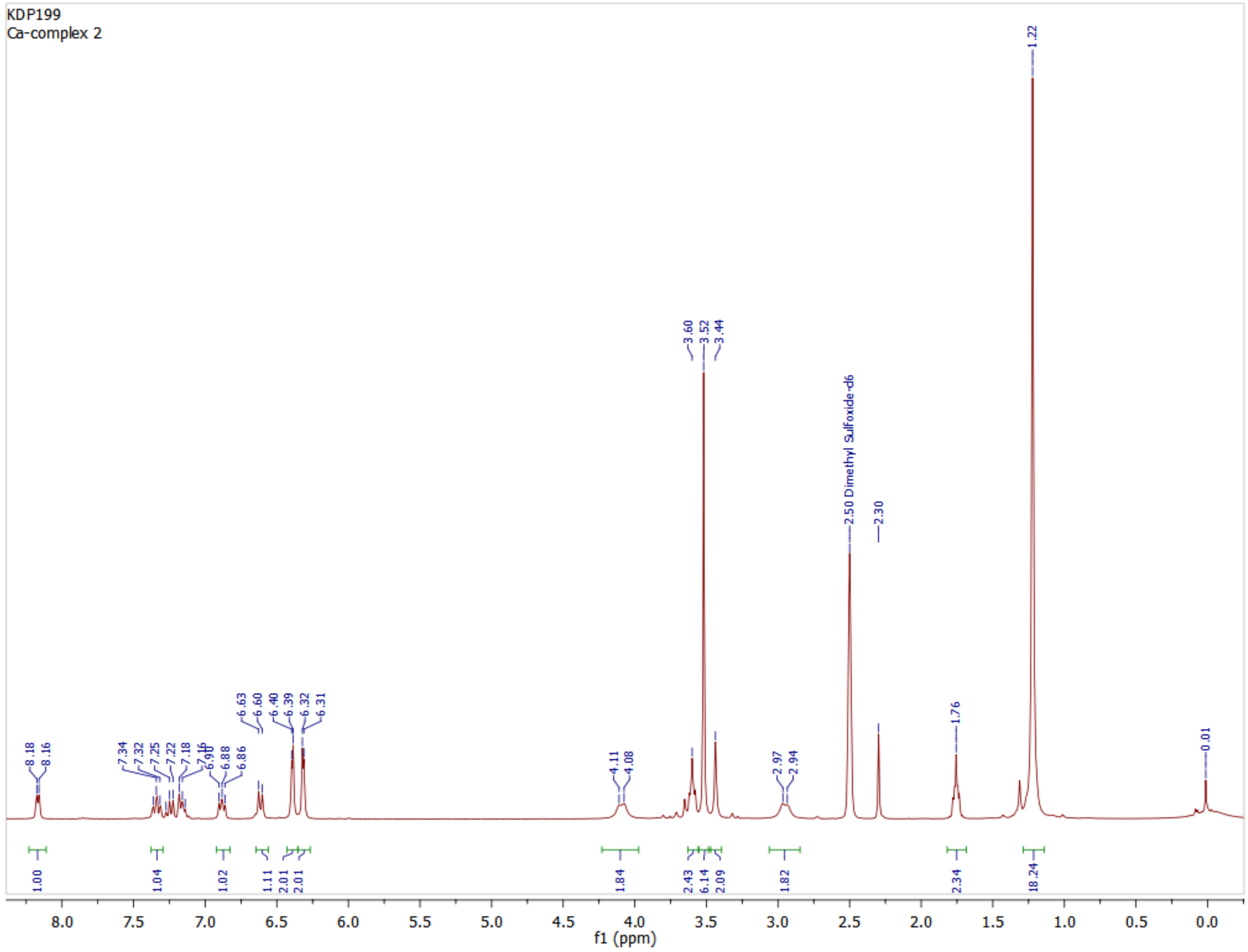

Fig. S27. ^{1}H NMR spectrum of **6** in DMSO-d_6 prepared via route B) in Scheme 1.

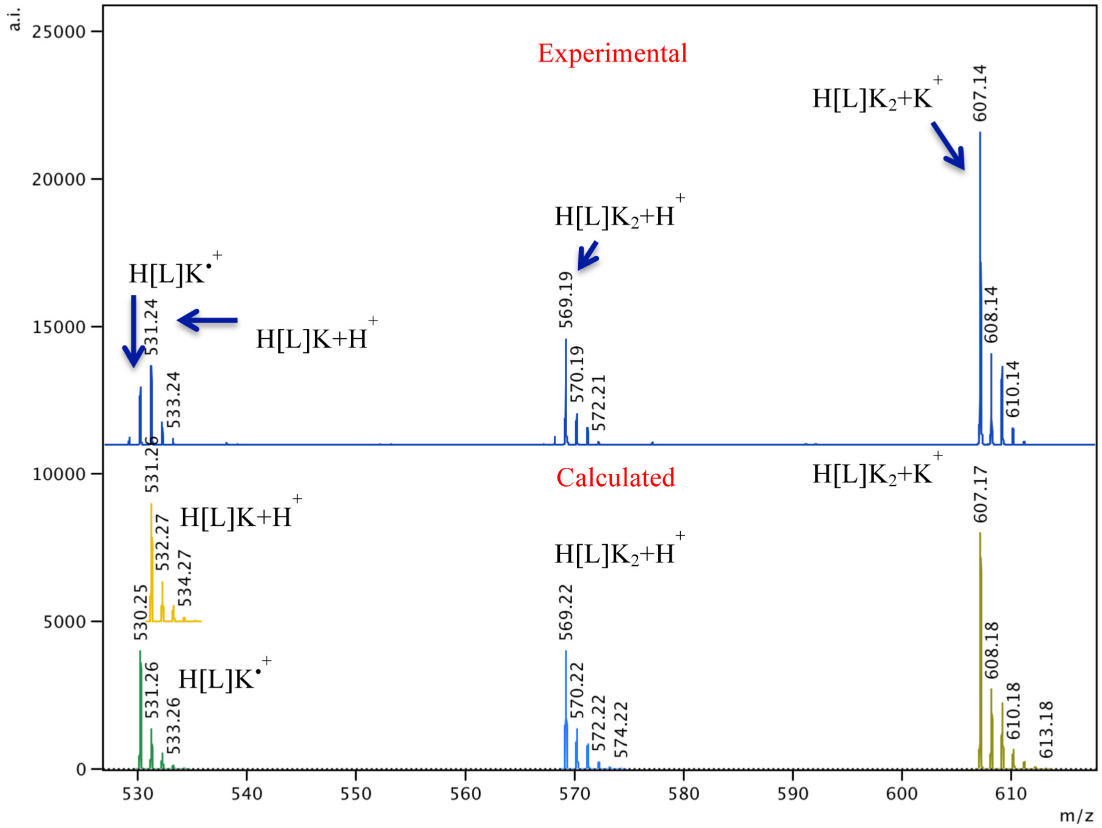

Figure S28. MALDI-TOF mass spectrum of **5** with calculated modeling isotopic distribution patterns.

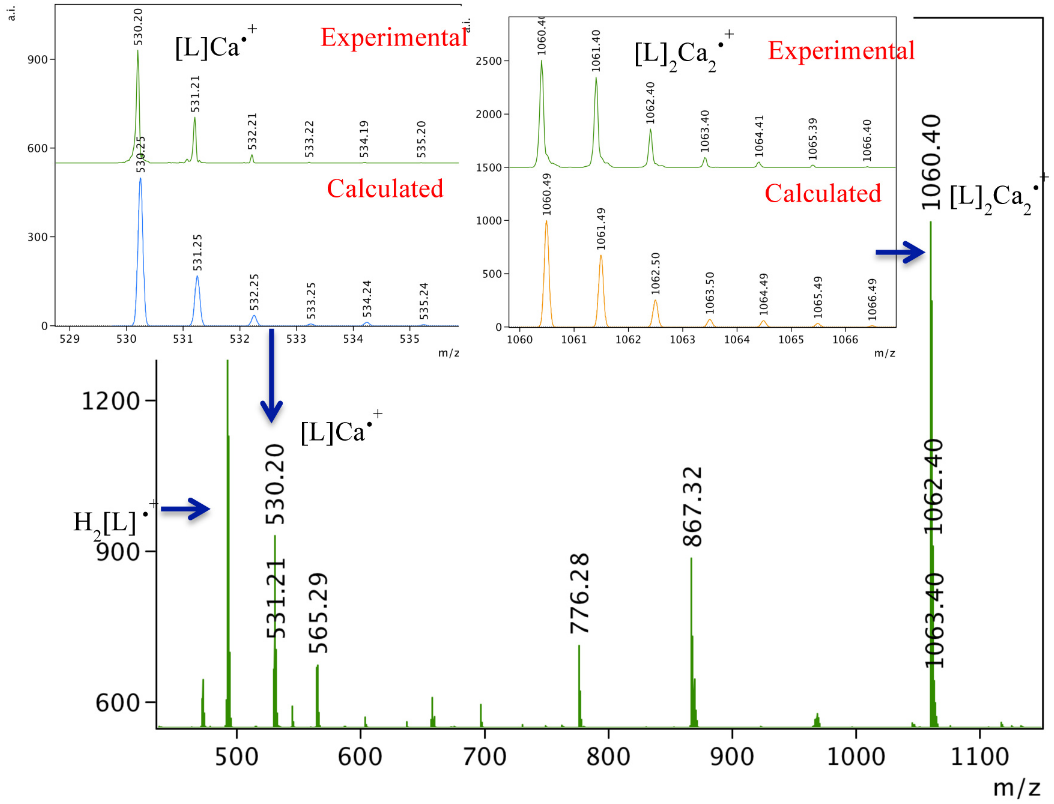

Figure S29. MALDI-TOF mass spectrum of **6** with calculated modeling isotopic distribution patterns.

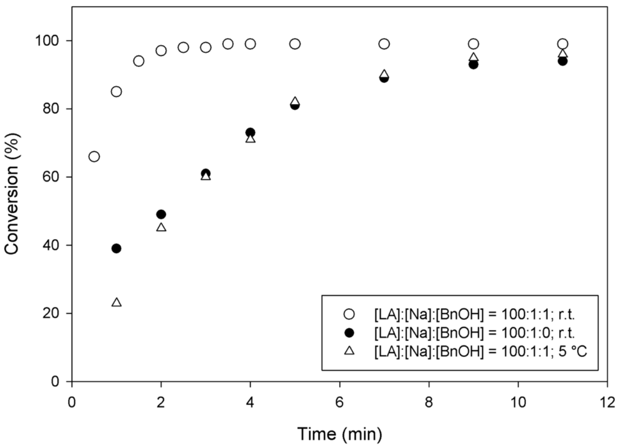

Figure S30. Conversion vs time plot of ROP of *rac*-lactide by **3**·THF in toluene. Conditions: [LA]:[Na]:[BnOH] = 100:1:1, 25 °C (r.t.) and 5 °C, and 100:1:0 at 25 °C.

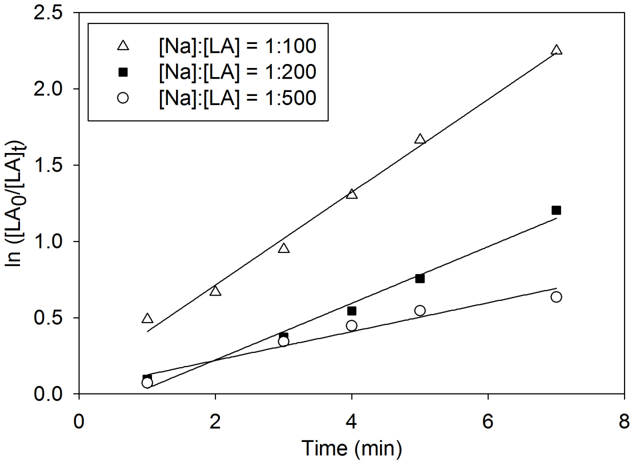

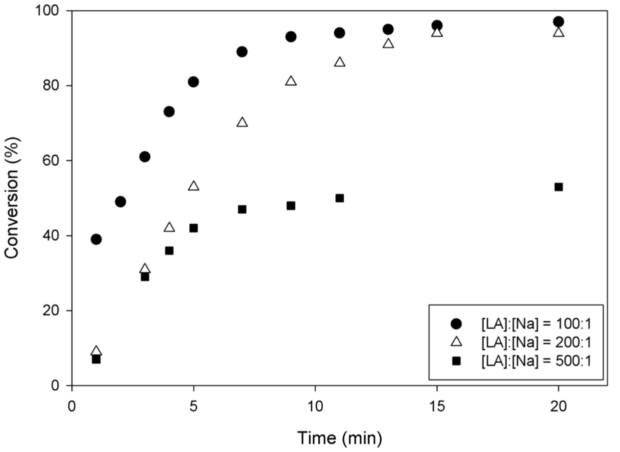

Figure S31. Plots of ln($[LA]_0/[LA]_t$) vs. time for ROP of *rac*-lactide by **3**·THF with different [LA]:[Na] ratios without BnOH at 25 °C in toluene (top). Conversion vs time of ROP of *rac*-lactide by **3**·THF at different [LA]:[Na] ratios without BnOH at r.t. in toluene (bottom).

Table S2. Observed reaction rates (k_{obs}) for the linear fits in Figures S31 and 5 for **3**·THF

Entry	[LA]:[Na]:[BnOH]	k_{obs} (min^{-1})
1	100:1:0	0.3044 ± 0.0128
2	200:1:0	0.1856 ± 0.0123
3	500:1:0	0.0945 ± 0.0119
4	100:1:1	1.6399 ± 0.0602
5	200:1:1	0.8717 ± 0.0312
6	500:1:1	0.0510 ± 0.0116

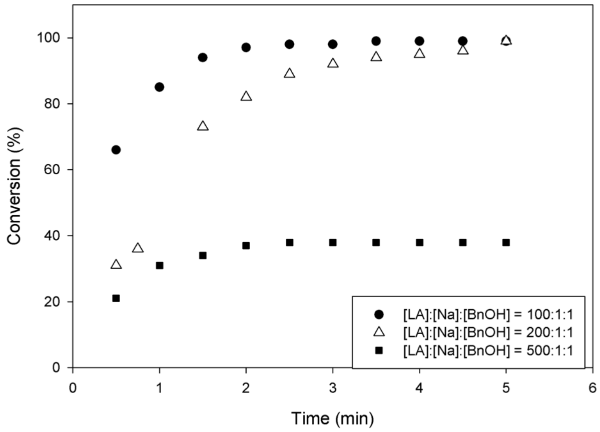

Figure S32. Conversion vs time plot of ROP of *rac*-lactide by **3**·THF at different [LA]:[Na] ratios with BnOH at r.t. in toluene.

Table S3. Observed reaction rates (k_{obs}) for the linear fits in Figure 7.

Entry	[LA]:[Na]:[BnOH]	Ratio	k_{obs} (min^{-1})
1	[LA]:[**3**·THF]:[BnOH]	100:1:0	0.299 ± 0.0154
2	[LA]:[**1**·THF]:[H_2**L**]:[BnOH]	100:0.5:0.5:0	0.0484 ± 0.00130
3	[LA]:[**3**·THF]:[BnOH]	100:1:1	1.46 ± 0.112
4	[LA]:[**1**·THF]:[H_2[**L**]]:[BnOH]	100:0.5:0.5:1	0.721 ± 0.0789

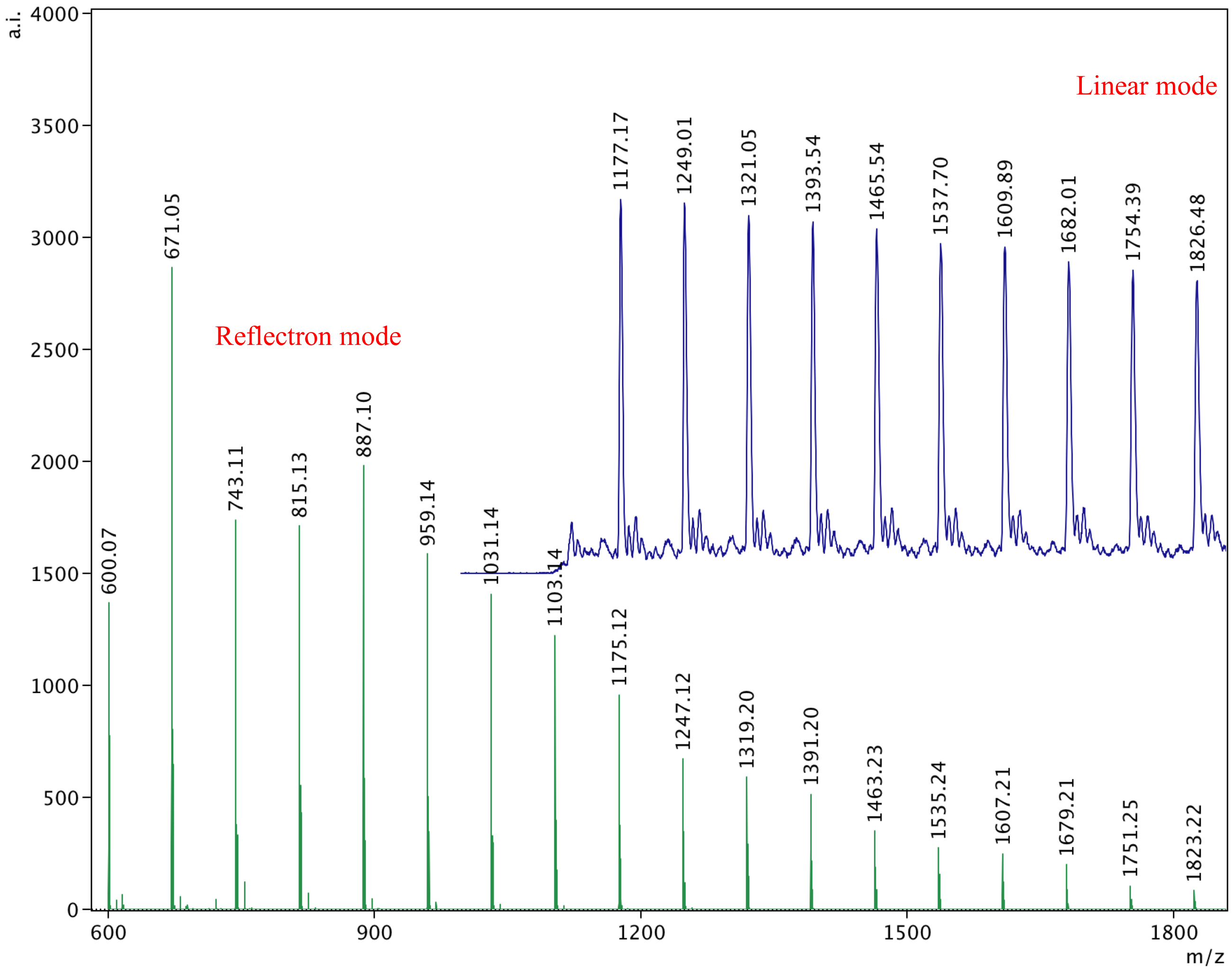

Figure S33. MALDI-TOF mass spectrum of the polymer produced according to the conditions in Table 4, entry 7. Reflectron mode (green) and linear mode (blue) spectra are in good agreement with each other.

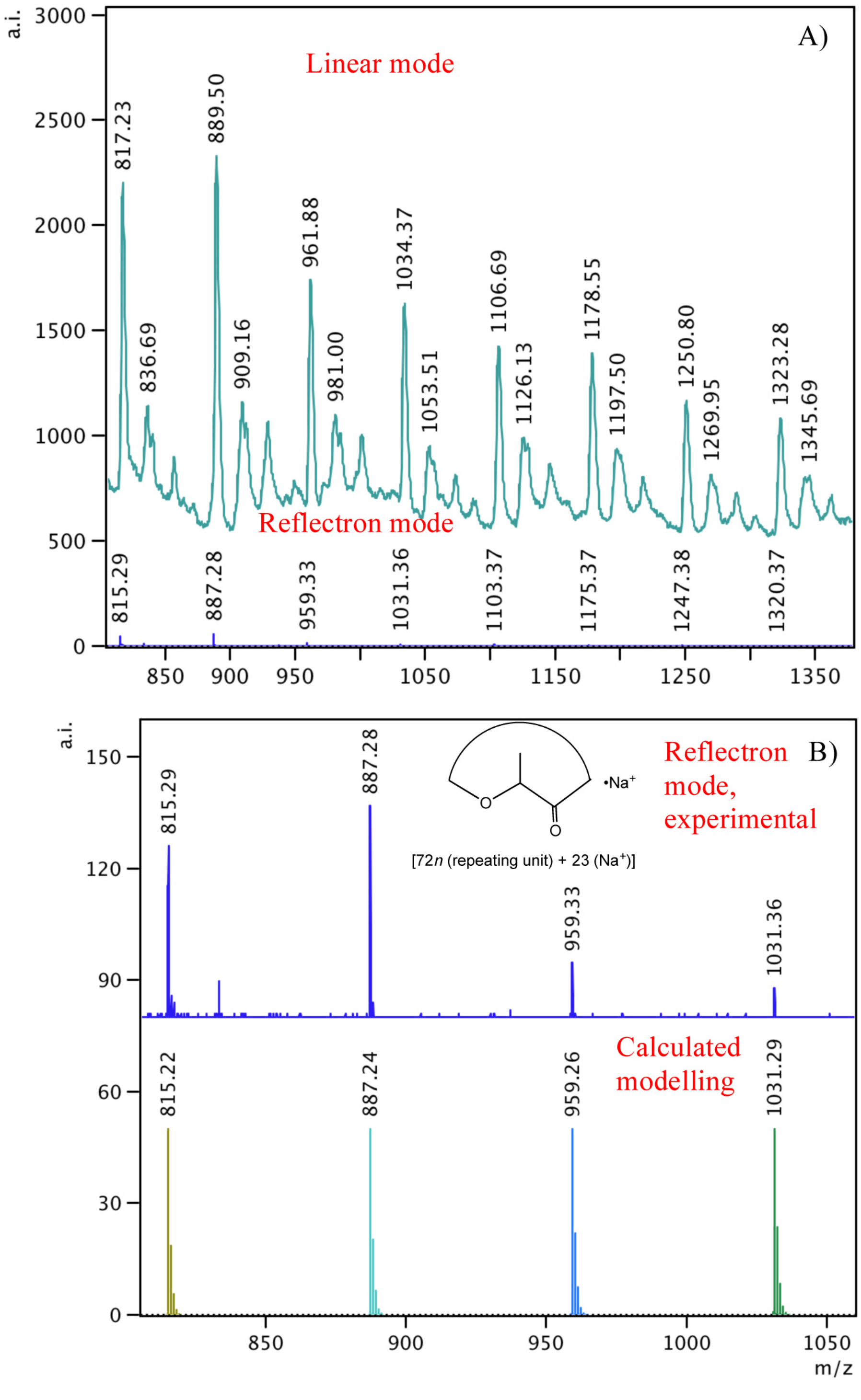

Figure S34. MALDI-TOF mass spectrum of the polymer produced according to the conditions in Table 4, entry 10. A) Linear (upper) vs. reflectron (lower) mode. B) Expanded section, *m/z* 800 – 1050 with calculated isotopic patterns and the possible structure of the polymer based on the calculation shown.

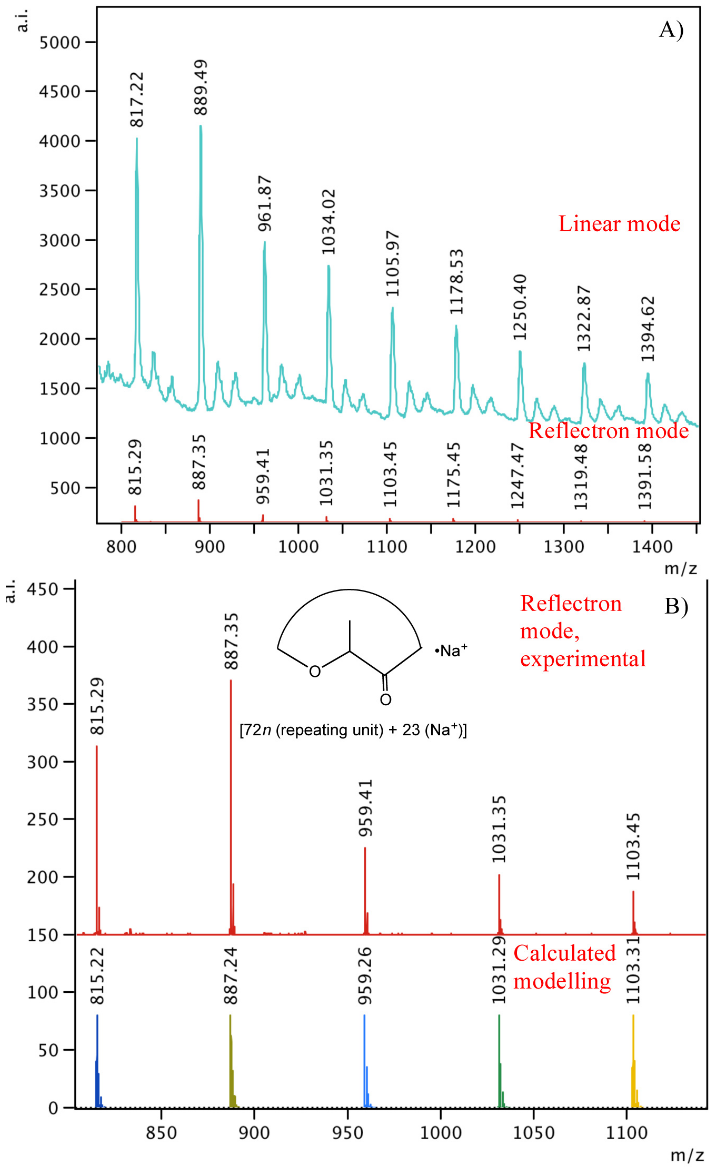

Figure S35. MALDI-TOF mass spectrum of the polymer produced according to the conditions in Table 4, entry 11. A) Linear (upper) vs. reflectron (lower) mode. B) Expanded section, *m/z* 800 – 1150 (upper) with calculated isotopic patterns (lower) and the possible structure of the polymer based on the calculation shown.

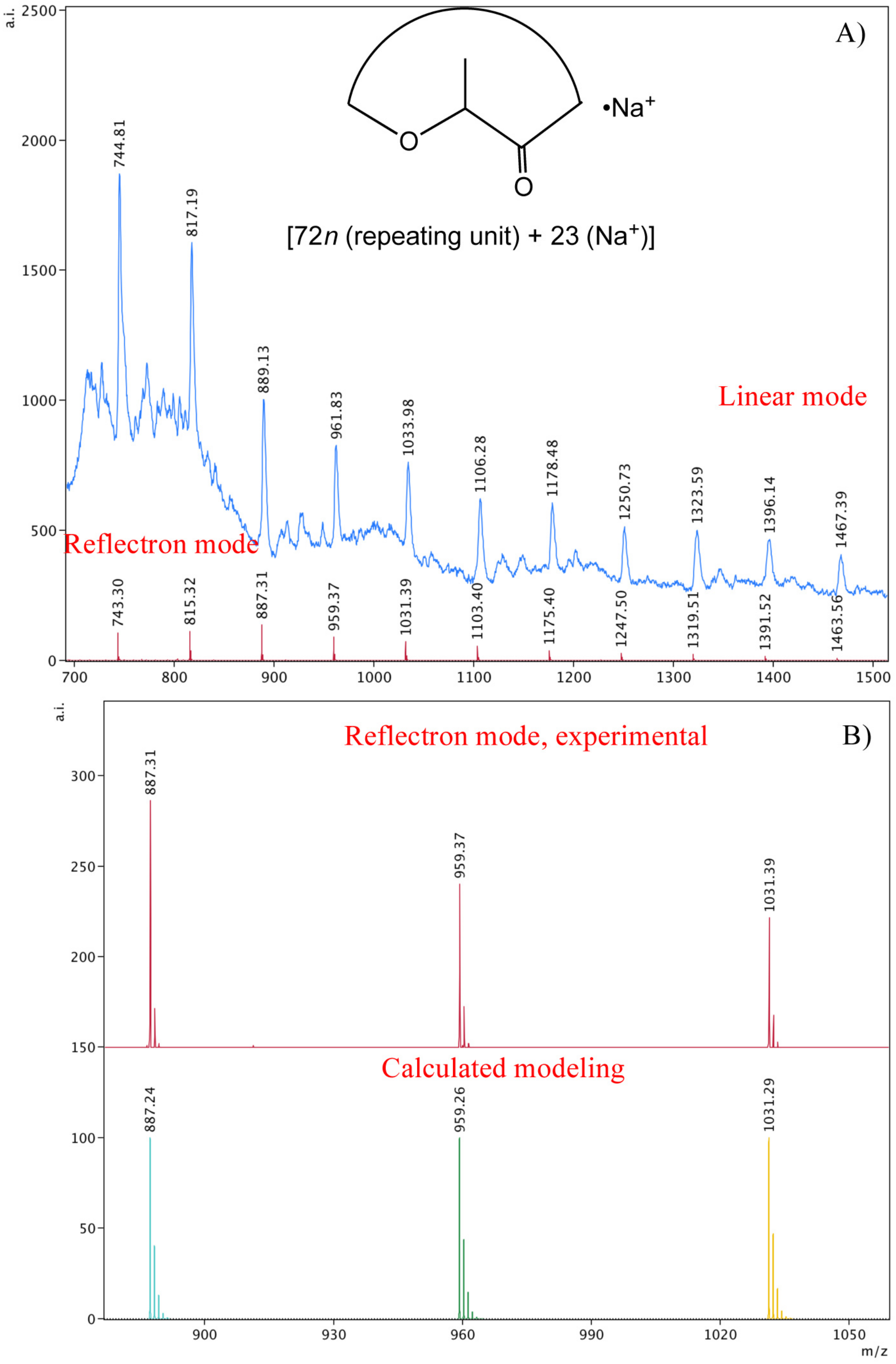

Figure S36. MALDI-TOF mass spectrum of the polymer produced by **1** + H_2[**L**] without BnOH, linear mode (upper) and reflectron mode (lower) with the possible structure of the polymer based on the calculation shown. B) Expanded section, *m/z* 800 – 1050 (upper) with calculated isotopic patterns (lower).

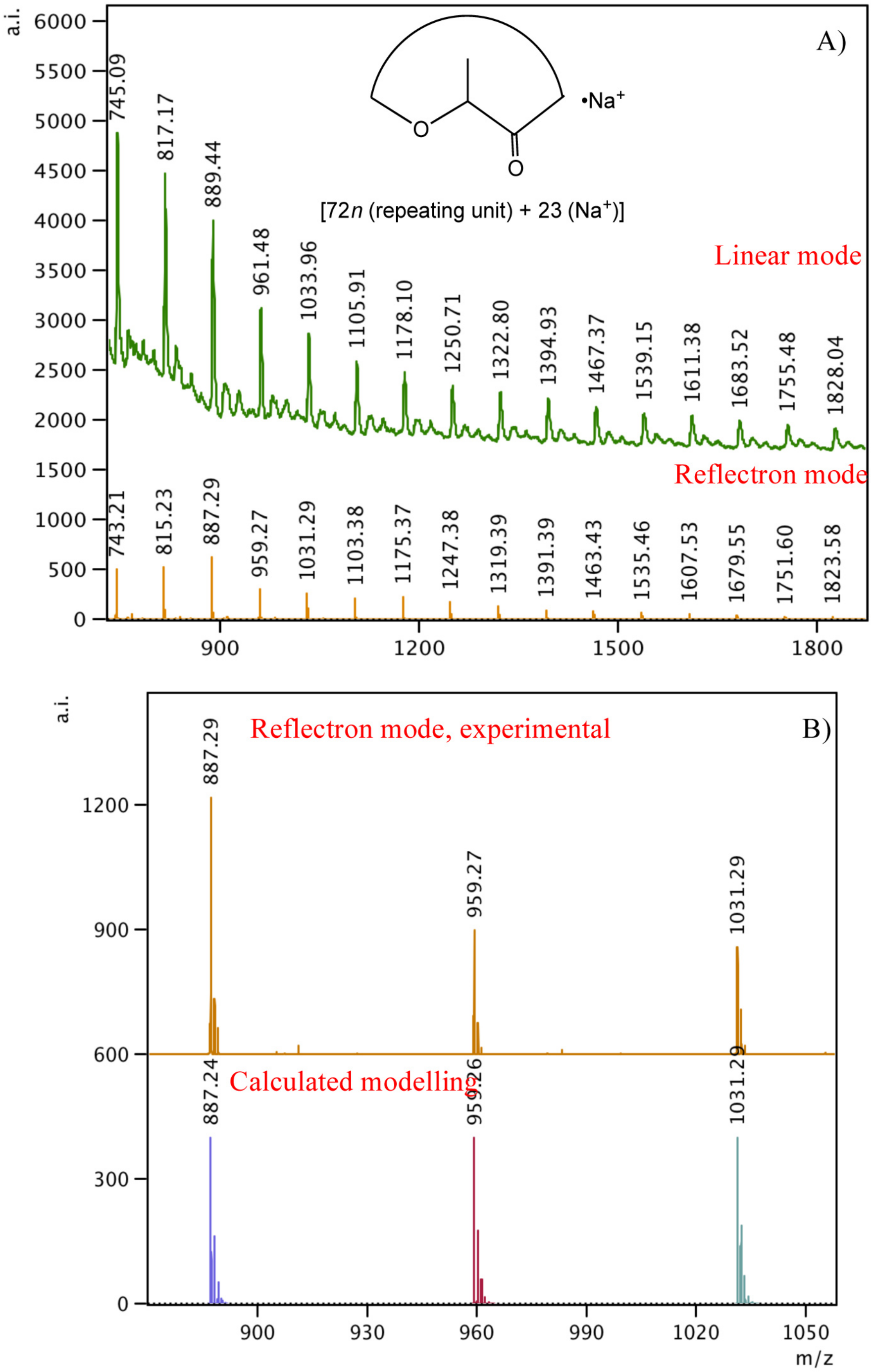

Figure S37. MALDI-TOF mass spectrum of the polymer produced by **1** + H_2[**L**] with BnOH, linear mode (upper) and reflectron mode (lower) with the possible structure of the polymer based on the calculation shown. B) Expanded section, *m/z* 800 – 1050 (upper) with calculated isotopic patterns (lower).

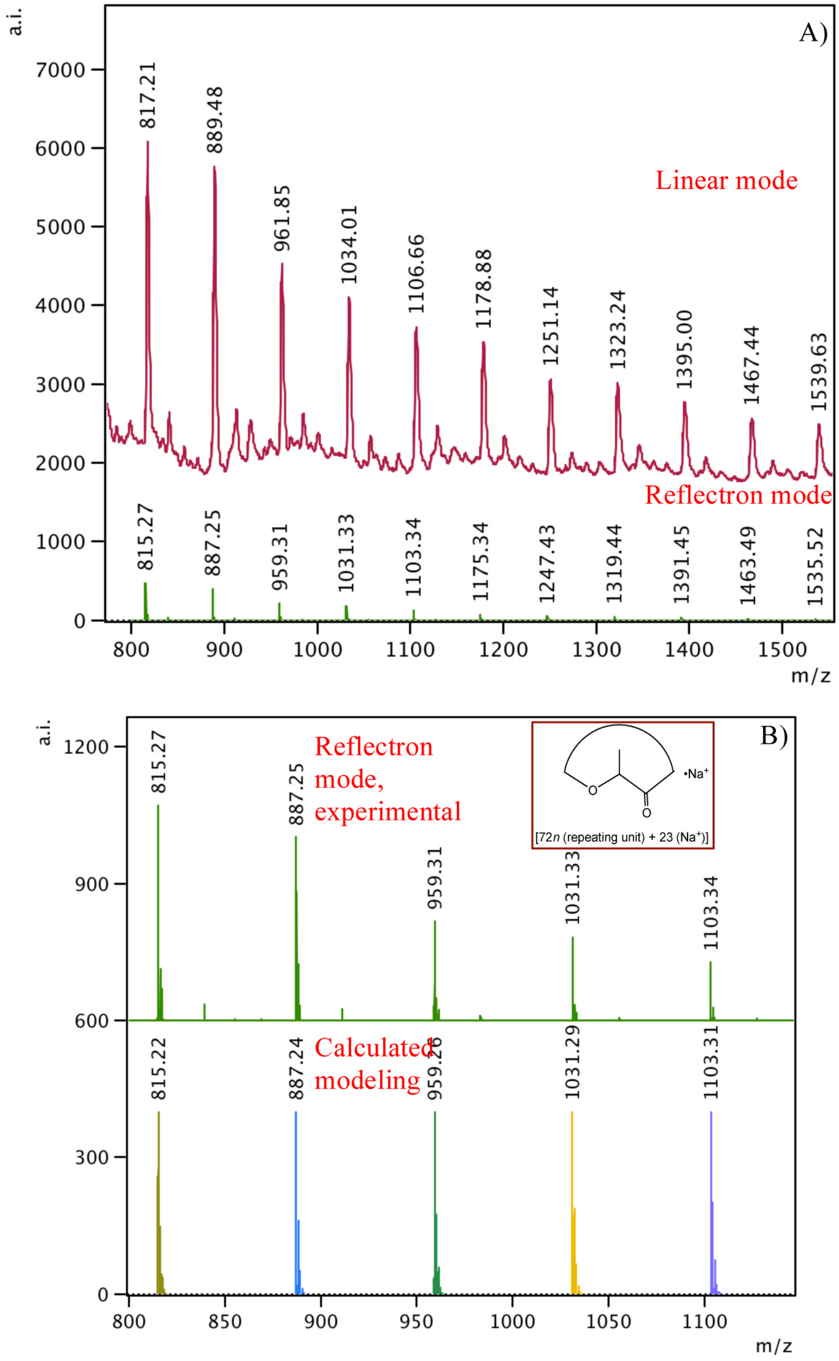

Figure S38. MALDI-TOF mass spectrum of the polymer produced according to the conditions in Table 4, entry 15. A) Linear (upper part) vs. reflectron (lower part) mode. B) Expanded section, *m/z* 800 – 1150 (upper part) with calculated isotopic patterns (lower part) and the possible structure of the polymer based on the calculation shown.

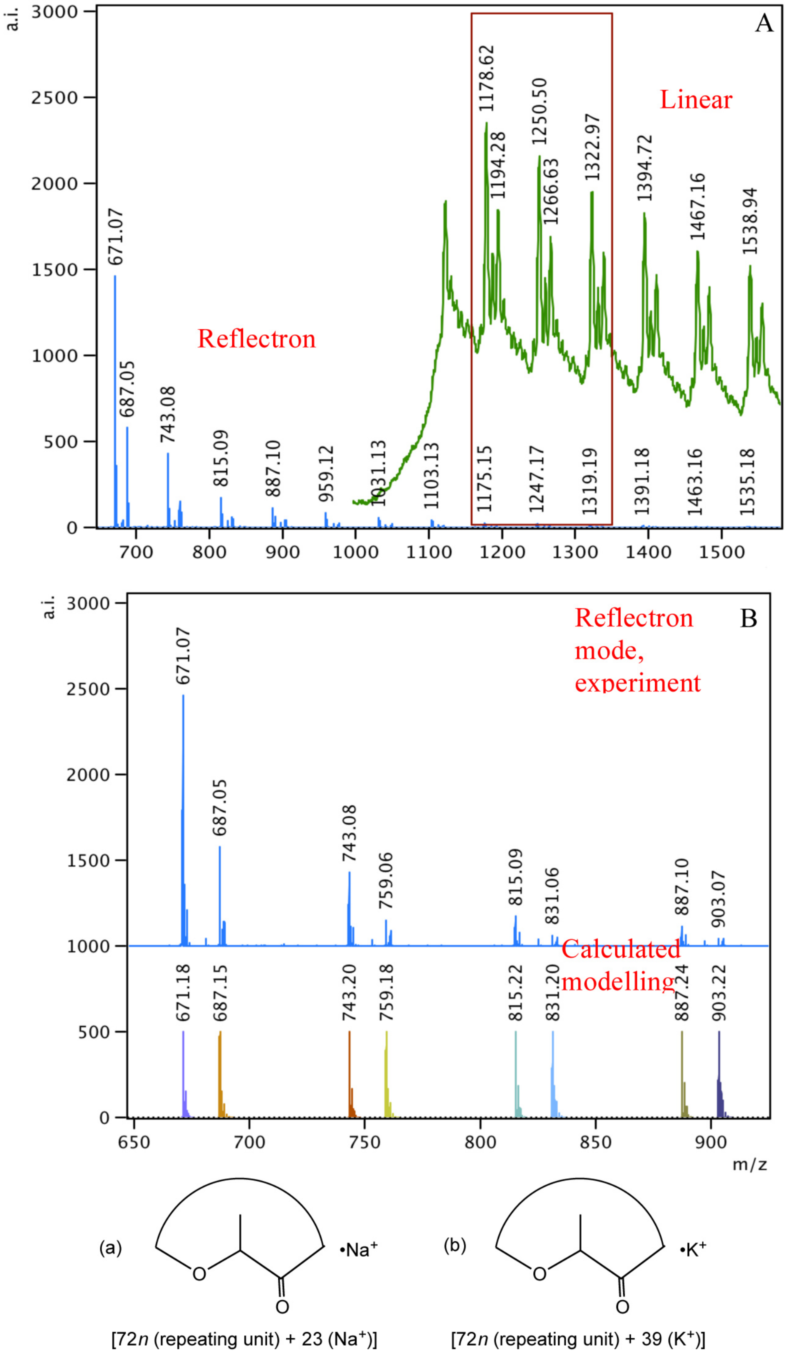

Figure S39. MALDI-TOF mass spectrum of the polymer produced according to the conditions in Table 4, entry 17. A) Linear (upper part) vs. reflectron (lower part) mode. B) Zoomed in section, *m/z* 650 – 950 (upper part) with calculated isotopic patterns (lower part) and the possible structures of the polymers based on the calculations shown.

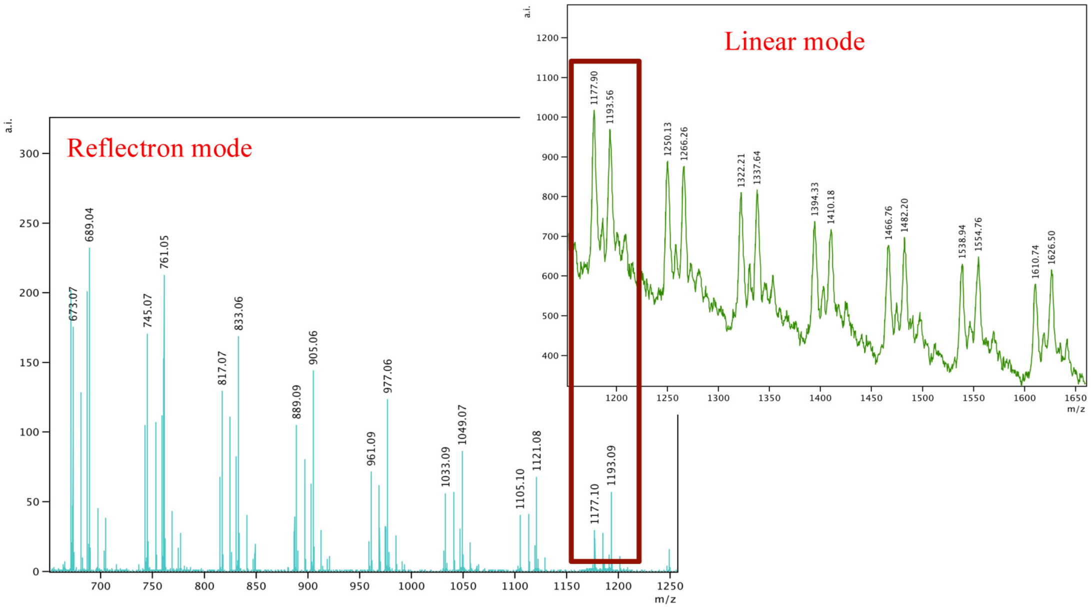

Figure S40. MALDI-TOF mass spectrum of the polymer produced according to the conditions in Table 4, entry 18. Reflectron mode (left side) and linear mode (right side) spectra are in good agreement with each other.

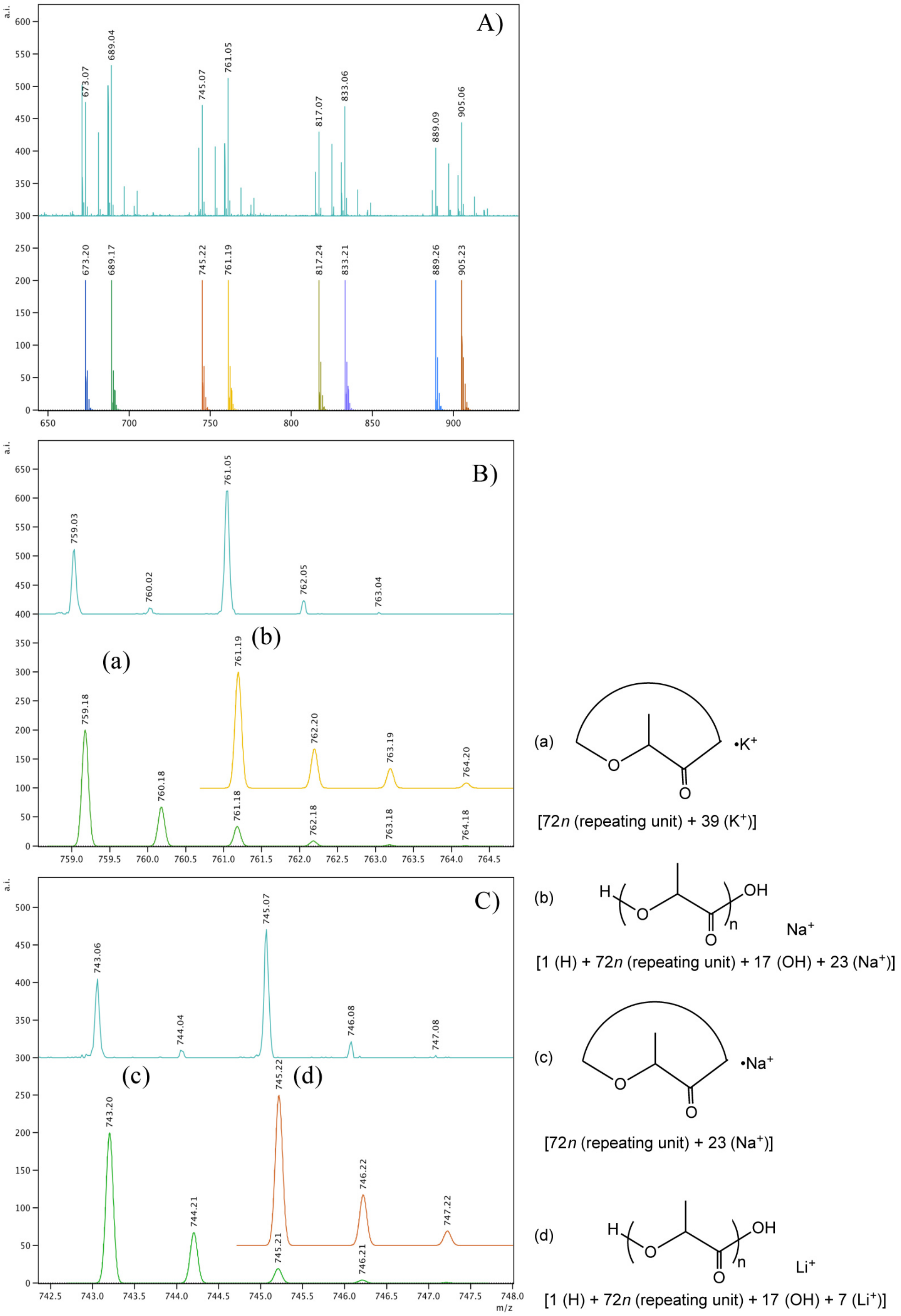

Figure S41. A) Expanded section of Figure S40, *m/z* 650 – 950. B) Calculated isotopic patterns for peaks *m/z* 759.03 (a) and 761.05 (b). C) Calculated isotopic patterns for peaks *m/z* 743.06 (c) and 745.07 (d) and the possible structures of the polymers based on the calculations shown.

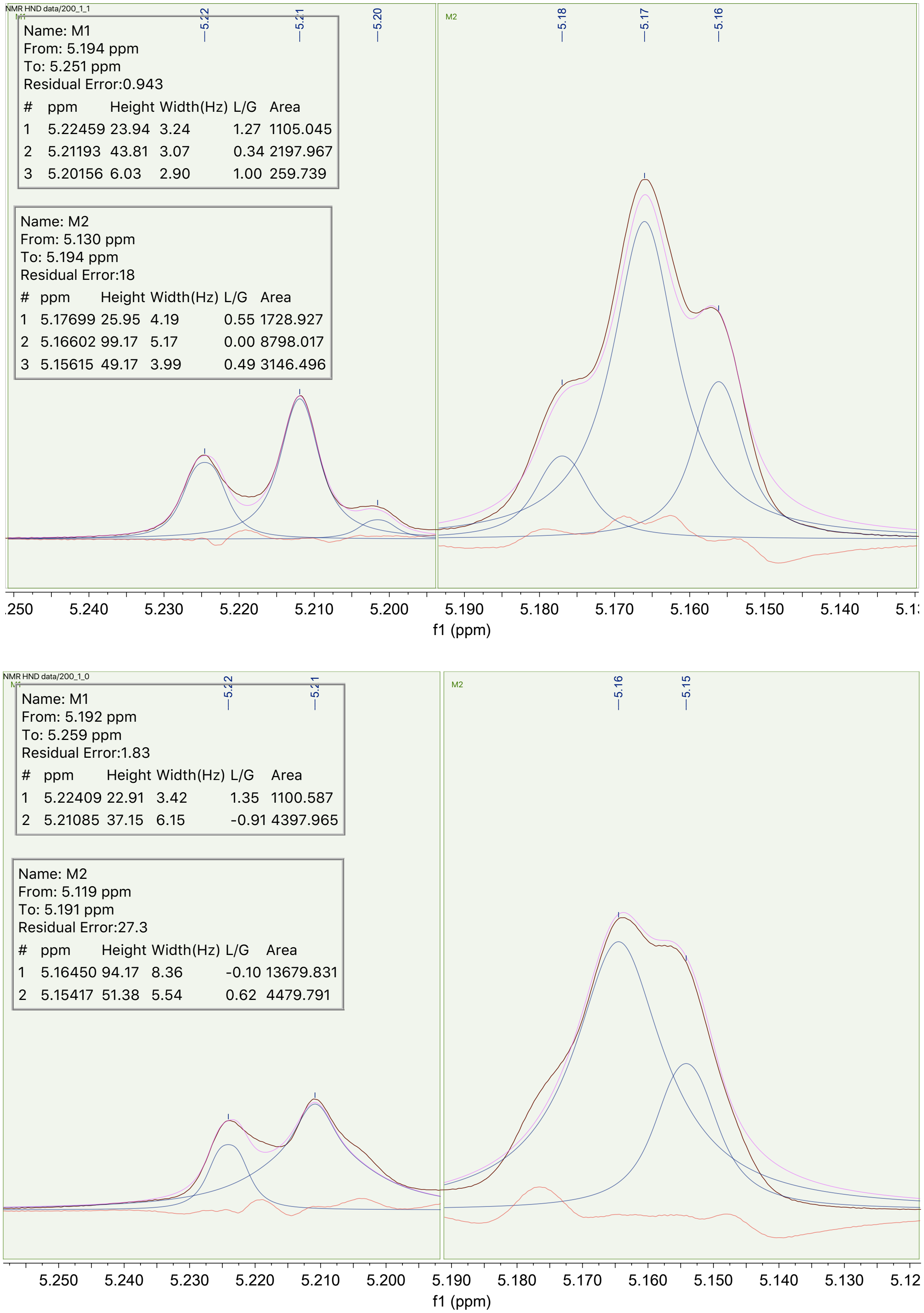

```
Name: M1
From: 5.194 ppm
To: 5.251 ppm
Residual Error:0.943
#   ppm       Height Width(Hz) L/G   Area
1   5.22459 23.94  3.24        1.27  1105.045
2   5.21193  43.81  3.07        0.34 2197.967
3   5.20156 6.03    2.90        1.00  259.739
```

```
Name: M2
From: 5.130 ppm
To: 5.194 ppm
Residual Error:18
#  ppm       Height Width(Hz) L/G   Area
1  5.17699 25.95  4.19        0.55 1728.927
2  5.16602 99.17  5.17        0.00 8798.017
3  5.15615  49.17  3.99        0.49 3146.496
```

```
Name: M1
From: 5.192 ppm
To: 5.259 ppm
Residual Error:1.83
#  ppm       Height Width(Hz) L/G    Area
1  5.22409 22.91  3.42       1.35   1100.587
2  5.21085 37.15  6.15       -0.91 4397.965
```

```
Name: M2
From: 5.119 ppm
To: 5.191 ppm
Residual Error:27.3
#  ppm       Height Width(Hz) L/G    Area
1  5.16450 94.17  8.36       -0.10 13679.831
2  5.15417  51.38  5.54       0.62   4479.791
```

Figure S42. ^{1}H{^{1}H} NMR spectrum (500 MHz, $CDCl_3$) of the methine region of PLA produced by $[LA]_0$:[**3**·THF$]_0$:$[BnOH]_0$ = 200:1:1 in toluene, Table 4 entry 8 (top), and by $[LA]_0$:[**3**·THF$]_0$:$[BnOH]_0$ = 200:1:0 in toluene, Table 4 entry 9 (bottom). $P_r = 2I_1/(I_1 + I_2)$, with I_1 = 5.20 – 5.25 ppm (rmr, mmr/rmm), I_2 = 5.13 – 5.20 ppm (mmr/rmm, mmm, mrm).

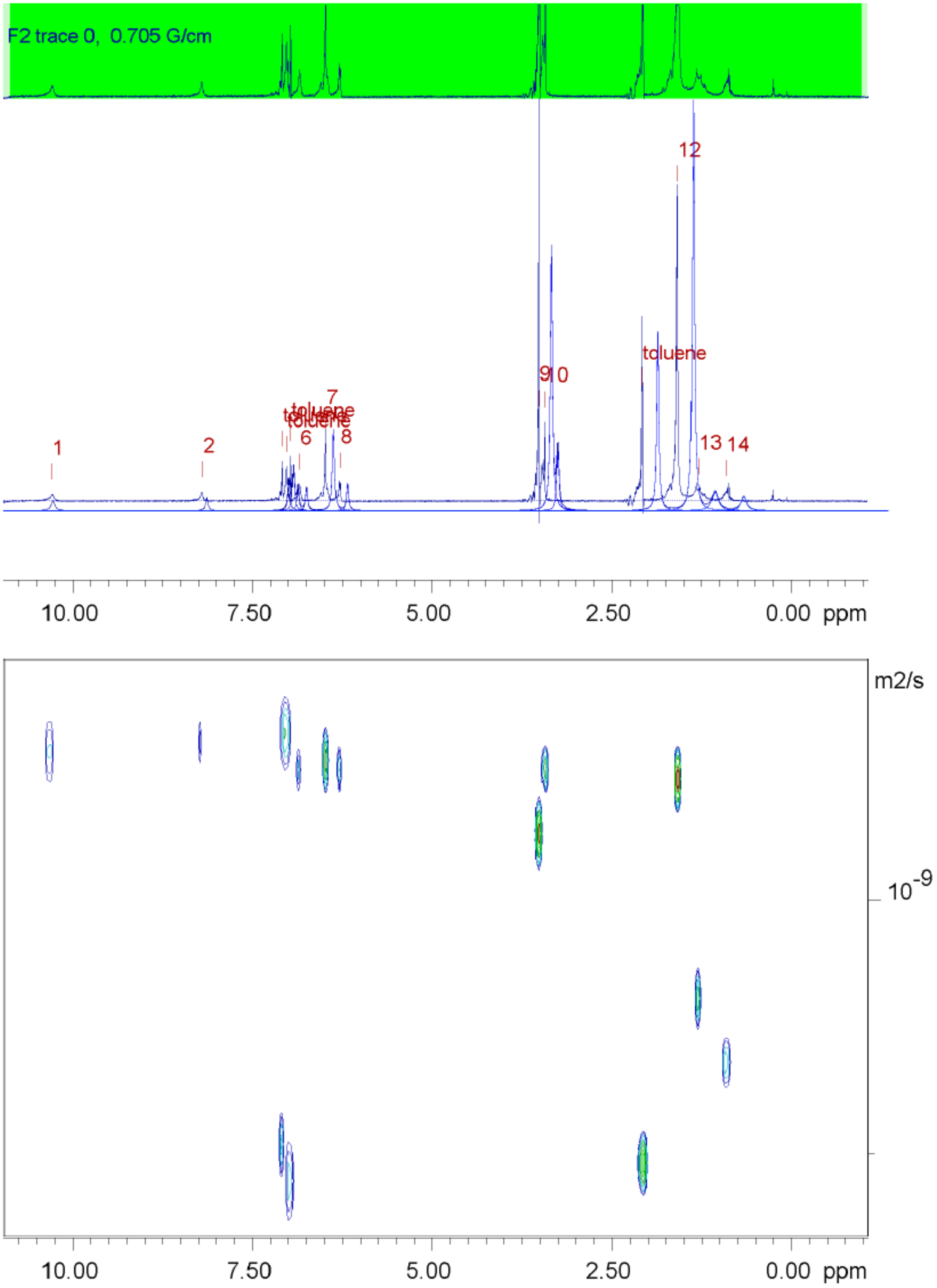

Figure S43. Diffusion analysis of **3**·THF via DOSY NMR spectroscopy.

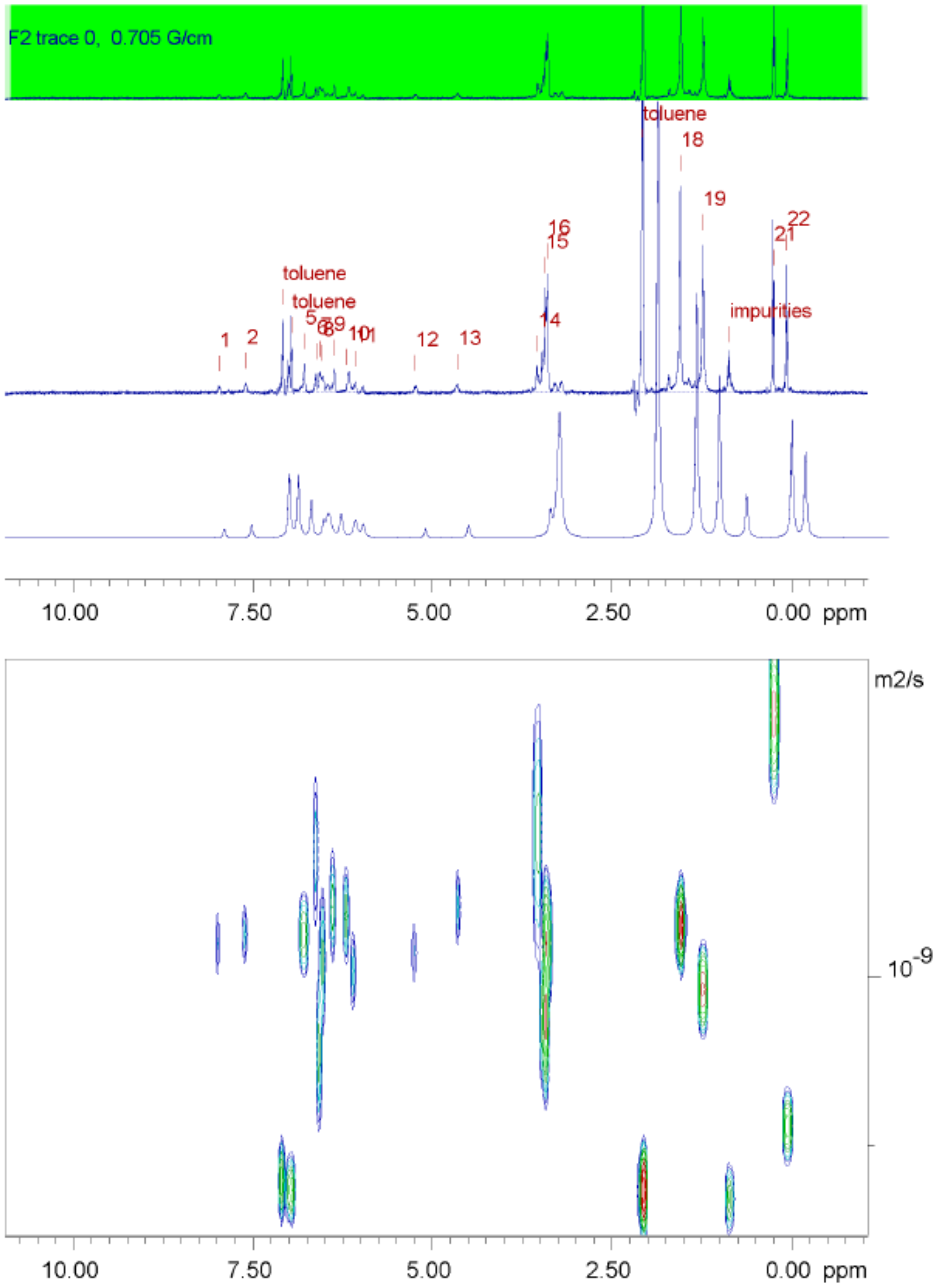

Figure S44. Diffusion analysis of **4** via DOSY NMR spectroscopy.

Table S4. Diffusion coefficients (D_t) and hydrodynamic radii of the complexes measured through DOSY measurements (r_H) and single crystal X-ray diffraction ($r_{X\text{-ray}}$)

Complex	D_t ($\times 10^{-10}$ m^2s^{-1})[a]	r_H (Å)[a]	$r_{X\text{-ray}}$ (Å)
3·THF	7.0801	4.860	5.905[b] (monomer) 7.440[b] (dimer) 11.48[c] (monomer) 10.97[c] (monomer no THF) 14.95[c] (dimer) 11.74[c] (dimer no THF)
4	8.7721	4.847	5.805[b] (monomer) 7.314[b] (dimer) 11.136[c] (monomer) 13.141[c] (dimer)

[a] Calculated hydrodynamic radii (r_H) from translational diffusion coefficients (D_t)

[b] Calculated from single crystal data using the equation $r_{X\text{-ray}} = (3V/4\pi n)^{1/3}$ where V is the volume of unit cell and n is the number of the compounds of interest occupying the unit cell assuming spherical shape. "Monomer" refers to the molecular formula unit and "dimer" refers to the hydrogen-bonded structure containing two formula units.

[c] Calculated from single crystal data according to $r_{X\text{-ray}} = (a^2b)^{1/3}$ where a and b are the major and minor semi-axes, respectively, of the oblate spheroid formed by the complex.